

Phase structure of many-flavor QED₃Jens Braun,^{1,2,3} Holger Gies,^{3,4} Lukas Janssen,^{5,3} and Dietrich Roscher^{1,3}¹*Institut für Kernphysik (Theoriezentrum), Technische Universität Darmstadt, D-64289 Darmstadt, Germany*²*ExtreMe Matter Institute EMMI, GSI, Planckstraße 1, D-64291 Darmstadt, Germany*³*Theoretisch-Physikalisches Institut, Abbe Center of Photonics, Friedrich-Schiller-Universität Jena, Max-Wien-Platz 1, D-07743 Jena, Germany*⁴*Helmholtz-Institut Jena, Fröbelstieg 3, D-07743 Jena, Germany*⁵*Department of Physics, Simon Fraser University, Burnaby, British Columbia V5A 1S6, Canada*

(Received 16 April 2014; published 7 August 2014)

We analyze the many-flavor phase diagram of quantum electrodynamics (QED) in $2 + 1$ (Euclidean) space-time dimensions. We compute the critical flavor number above which the theory is in the quasiconformal massless phase. For this, we study the renormalization group fixed-point structure in the space of gauge interactions and pointlike fermionic self-interactions, the latter of which are induced dynamically by fermion-photon interactions. We find that a reliable estimate of the critical flavor number crucially relies on a careful treatment of the Fierz ambiguity in the fermionic sector. Using a Fierz-complete basis, our results indicate that the phase transition towards a chirally broken phase occurring at small flavor numbers could be separated from the quasiconformal phase at larger flavor numbers, allowing for an intermediate phase which is dominated by fluctuations in a vector channel. If these interactions approach criticality, the intermediate phase could be characterized by a Lorentz-breaking vector condensate.

DOI: [10.1103/PhysRevD.90.036002](https://doi.org/10.1103/PhysRevD.90.036002)

PACS numbers: 12.20.-m, 11.10.Kk, 11.15.Tk

I. INTRODUCTION

The competition between screening and antiscreening effects is at the heart of the intriguing diversity of phases occurring in asymptotically free theories. Not only thermal phase transitions governed by parameters such as temperature or chemical potentials, but also quantum phase transitions triggered by the number of active degrees of freedom have recently been of central interest. Most prominently, the number of light fermion degrees of freedom N_f often serves as a control parameter to tune the screening–antiscreening competition. While chiral quantum phase transitions of this type have attracted considerable attention in four-dimensional non-Abelian gauge theories because of their potential relevance for embeddings of the Higgs sector in beyond-standard-model scenarios [1–7], similar theoretical mechanisms can be at work in the Abelian theory of quantum electrodynamics (QED) in $d = 3$ (Euclidean) spacetime dimensions. Beyond the predominantly conceptual interest, such studies gain significance from layered condensed-matter systems for which $d = 2 + 1$ dimensional QED with four-component Dirac fermions can serve as an effective field theory for low-energy excitations. Applications of this type have been discussed, e.g., in the context of graphene, surface states of three-dimensional topological insulators, and high-temperature cuprate superconductors. For recent reviews on this rapidly evolving field, see, e.g., Refs. [8,9]. In particular, QED₃ has been proposed to model the destruction of phase coherence in the underdoped cuprates [10–16]. Chiral symmetry breaking in QED₃ then describes the

zero-temperature transition from the d -wave superconducting state into the antiferromagnetic state. The size of the dynamically generated mass in the effective theory consequently determines the band gap in the insulating phase of the underdoped cuprates.

As the coupling constant of QED₃ has a positive mass dimension, the theory is asymptotically free for purely dimensional reasons: any finite value of the coupling, if measured in terms of a reference scale, will become arbitrarily small if this reference scale is pushed to asymptotically large energies or momenta. In turn, one expects QED₃ to become more strongly coupled at low energies, possibly generating fermion masses through a chiral phase transition. By contrast, increasing the number of fermion flavors enhances the screening properties of fermionic fluctuations. If this screening dominates, the coupling may remain small and the theory can be expected to be in the disordered massless phase. More precisely, the fluctuations can generate an infrared (IR) fixed point, such that the theory remains quasiconformal: it has a nontrivial RG flow from the Gaussian ultraviolet (UV) to the IR fixed point with the transition scale set by the dimensionful gauge coupling. Scenarios of this type have been suggested and analyzed in many works, and the critical flavor number $N_{f,\text{cr}}^\gamma$ separating the chirally broken phase for small N_f from the symmetric for large N_f has been estimated by a variety of nonperturbative methods; see, e.g., Refs. [17–40]. Predictions from self-consistent approximations of the Dyson-Schwinger equations (DSE) in their most advanced form yield results near $N_{f,\text{cr}}^\gamma \approx 4$; see, e.g., [28]. Recently,

these studies have been extended to incorporate lattice anisotropies as well as finite temperature in order to approach more realistic applications [41–44]. An early RG study found $N_{f,cr}^Z \approx 3.1$ [30]. Based on a thermodynamic argument an inequality $N_{f,cr}^Z \leq 1.5$ has been conjectured [26], but was challenged later [15]. Another upper bound $N_{f,cr}^Z < 7$ has been claimed recently using an RG monotonicity argument [40]. On the other hand, lattice simulations in QED₃ are difficult due to a large separation of scales; however, they appear to agree at least on a lower bound $N_{f,cr}^Z > 1$ [32,33,35,37]. The actual value of $N_{f,cr}^Z$ in QED₃ is in fact of profound interest for the effective cuprate models, in which the number of four-component Dirac flavors is $N_f = 2$: If $N_{f,cr}^Z > 2$, then the effective theory predicts a direct transition from the d -wave superconducting into the antiferromagnetic phase at $T = 0$ as a function of the doping [12,13]. Otherwise, a small $N_{f,cr}^Z < 2$ would leave the possibility of an unconventional non-Fermi-liquid phase in the $T = 0$ underdoped cuprates [10,11,14].

In the present work, we take a fresh look at the phase structure of QED₃ as a function of the fermion number. We pay particular attention to all interaction channels allowed by the large $U(2N_f)$ flavor symmetry for Dirac fermions in the reducible representation. Using the functional renormalization group (RG), we find evidence for a more involved structure of the phase diagram. Within our approach, we can straightforwardly identify the “conformal-critical” flavor number $N_{f,cr}^{qc}$ above which the theory is in the quasiconformal phase. *A priori*, $N_{f,cr}^{qc}$ can be different from the “chiral-critical” flavor number $N_{f,cr}^Z$ below which the theory is in the chirally broken phase. Our results suggest that $N_{f,cr}^Z \lesssim N_{f,cr}^{qc}$. This includes the interesting possibility of a third intermediate phase with N_f fermion flavors such that $N_{f,cr}^Z < N_f < N_{f,cr}^{qc}$. Our findings suggest that this phase is dominated by vector-channel fluctuations. If they become critical, the model features a Lorentz-breaking vector condensate and a correspondingly mixed spectrum of photonlike massless Goldstone bosons and massive excitations.

The present work is organized as follows: In Sec. II, we discuss the symmetries and fermionic interaction channels of QED₃. Corresponding symmetry-breaking patterns are briefly outlined in Sec. III. In Sec. IV, we introduce and apply the functional RG as our central technical tool in order to derive the RG flow equations for the interactions and wave-function renormalizations. Section V is devoted to a fixed-point analysis as a means to identify possible phase structures. An estimate of the conformal-critical flavor number $N_{f,cr}^{qc}$ marking the transition to the disordered quasiconformal phase is performed in Sec. VI. After illustrating the importance of Fierz completeness of the fermionic interaction channels in Sec. VII, we summarize our findings in the form of a conjectured phase diagram in Sec. VIII and conclude in Sec. IX. Some technical details are summed up in the Appendices.

II. SYMMETRIES AND FERMIONIC INTERACTION CHANNELS

Let us first recapitulate the flavor symmetries of QED₃ with many flavors, paying attention to the diversity of interaction channels; see [45,46] for an extended discussion.

The microscopic (classical) action of QED₃ with N_f fermion flavors in $d = 3$ Euclidean space-time is given by

$$S = \int d^3x \left\{ \bar{\psi}^a i \partial \psi^a + \bar{e} \bar{\psi}^a A \psi^a + \frac{1}{4} F_{\mu\nu} F^{\mu\nu} \right\}, \quad (1)$$

where \bar{e} denotes the bare dimensionful gauge coupling and summation over flavor indices a is tacitly assumed. The fermions $\psi, \bar{\psi}$ are considered to be four-component Dirac spinors, naturally occurring, e.g., in effective theories for electrons on a honeycomb lattice [47–53] or in cuprates [10–16]. They transform under a reducible representation of the Dirac algebra $\{\gamma_\mu, \gamma_\nu\} = 2\delta_{\mu\nu}$ in terms of 4×4 Dirac matrices

$$\gamma_\mu = \begin{pmatrix} 0 & -i\sigma_\mu \\ i\sigma_\mu & 0 \end{pmatrix}, \quad \mu = 1, 2, 3, \quad (2)$$

where $\{\sigma_\mu\}_{\mu=1,2,3}$ denote the standard Pauli matrices. The Clifford algebra can be spanned with the aid of two further 4×4 matrices

$$\gamma_4 = \begin{pmatrix} 0 & \mathbb{1}_2 \\ \mathbb{1}_2 & 0 \end{pmatrix} \quad \text{and} \quad \gamma_5 = \gamma_1 \gamma_2 \gamma_3 \gamma_4 = \begin{pmatrix} \mathbb{1}_2 & 0 \\ 0 & -\mathbb{1}_2 \end{pmatrix}, \quad (3)$$

which anticommute with each other as well as with all γ_μ . A complete Clifford basis is given by

$$\{\gamma_A\}_{A=1,\dots,16} = \{\mathbb{1}_4, \gamma_\mu, \gamma_4, \gamma_{\mu\nu}, i\gamma_\mu \gamma_4, i\gamma_\mu \gamma_5, \gamma_{45}, \gamma_5\}, \quad (4)$$

where $\gamma_{45} = i\gamma_4 \gamma_5$ and $\gamma_{\mu\nu} = \frac{i}{2} [\gamma_\mu, \gamma_\nu]$ [in Eq. (4), only those $\gamma_{\mu\nu}$ with $\mu < \nu$ are counted as independent].

The obvious $U(N_f)$ flavor symmetry of Eq. (1) together with rotations in the space of irreducible subcomponents of the Dirac spinors leads to an enhanced $U(2N_f)$ flavor (or “chiral”) symmetry of QED₃; see Appendix A for details.

From a renormalization group perspective, it is convenient to view the approach from the microscopic theory towards possible symmetry-broken regimes as a two-stage process: first, fluctuations involving gauge-fermion interactions induce effective fermionic self-interactions. Second, further fluctuations may lead to a rapid growth of the fermionic interactions driving the system to criticality and giving rise to possible condensation phenomena.

In the present work, we study the fermionic self-interactions in the pointlike (i.e., the zero-momentum) limit. To this end, we first classify all possible fermionic self-interactions which are compatible with the $U(2N_f)$

flavor symmetry as well as with the discrete C , P , and T symmetries of the model. Following [29,30,45,46,49], these interactions are given by the flavor-singlet channels

$$(V)^2 = (\bar{\psi}^a \gamma_\mu \psi^a)^2, \quad (P)^2 = (\bar{\psi}^a \gamma_{45} \psi^a)^2, \quad (5)$$

and the flavor-nonsinglet channels

$$(S)^2 = (\bar{\psi}^a \psi^b)^2 - (\bar{\psi}^a \gamma_4 \psi^b)^2 - (\bar{\psi}^a \gamma_5 \psi^b)^2 + (\bar{\psi}^a \gamma_{45} \psi^b)^2, \quad (6)$$

$$(A)^2 = (\bar{\psi}^a \gamma_\mu \psi^b)^2 + \frac{1}{2} (\bar{\psi}^a \gamma_{\mu\nu} \psi^b)^2 - (\bar{\psi}^a i \gamma_\mu \gamma_4 \psi^b)^2 - (\bar{\psi}^a i \gamma_\mu \gamma_5 \psi^b)^2. \quad (7)$$

Here, we have used the convention $(\bar{\psi}^a \psi^b)^2 \equiv \bar{\psi}^a \psi^b \bar{\psi}^b \psi^a$, etc. The corresponding 4-point correlation functions of these fermion interactions can develop largely independent structures in momentum space. By contrast, in the zero-momentum (pointlike) limit, these four-fermion interactions are connected due to Fierz identities,

$$(V)^2 + (S)^2 + (P)^2 = 0, \quad -4(V)^2 - 3(S)^2 + (A)^2 = 0. \quad (8)$$

In this limit, only two four-fermion terms are linearly independent. We choose to work with the flavor singlets and parametrize the corresponding part of the (effective) Lagrangian as

$$\begin{aligned} \mathcal{L}_{\psi,\text{int}} &= \frac{\bar{g}}{2N_f} (V)^2 + \frac{\tilde{g}}{2N_f} (P)^2 \\ &= \frac{\bar{g}}{2N_f} (\bar{\psi}^a \gamma_\mu \psi^a)^2 + \frac{\tilde{g}}{2N_f} (\bar{\psi}^a \gamma_{45} \psi^a)^2, \end{aligned} \quad (9)$$

with the bare couplings \bar{g} , \tilde{g} . In our RG study below, \bar{g} and \tilde{g} are set to zero at the initial scale. However, they can be generated dynamically during the RG flow. In any case, the first term $\sim \bar{g}$ corresponds to the interaction known from the Thirring model, whereas the second one $\sim \tilde{g}$ is similar to a Gross-Neveu interaction.¹

For $N_f > 1$, another Fierz basis may be of interest from a physical point of view:

$$\mathcal{L}_{\psi,\text{int}} = -\frac{\bar{g}_V}{2N_f} (V)^2 + \frac{\bar{g}_\phi}{4N_f} (S)^2, \quad (10)$$

where the couplings are related to those of Eq. (9) by

$$\begin{aligned} \bar{g}_V &= \tilde{g} - \bar{g}, \\ \bar{g}_\phi &= -2\tilde{g}. \end{aligned} \quad (11)$$

¹If expressed in terms of two-component Weyl spinors, this interaction is indeed identical to the Gross-Neveu interaction; cf. Appendix A.

In addition to the vector (Thirring) channel $\sim (V)^2$, we encounter the nonsinglet channel $\sim (S)^2$ of Eq. (6) reminiscent to the Nambu–Jona-Lasinio (NJL) model. We emphasize that the description of the system in terms of Eq. (9) is completely equivalent to that of Eq. (10) in the pointlike limit. The same is true for any other combination of two linearly independent (“Fierz-complete”) interactions out of the four channels $(V)^2$, $(P)^2$, $(S)^2$, or $(A)^2$.

We conclude this section by critically assessing the pointlike limit: from a more general viewpoint, pointlike interactions are only a special limit of fermionic correlation functions $\Gamma^{(n)}$, i.e.,

$$\begin{aligned} g_{\mathcal{O}}(\bar{\psi} \mathcal{O} \psi)^2 \\ = \lim_{p_i \rightarrow 0} \bar{\psi}^a(p_1) \bar{\psi}^b(p_2) \Gamma_{\mathcal{O}}^{(4),abcd}(p_1, p_2, p_3, p_4) \psi^c(p_3) \psi^d(p_4). \end{aligned} \quad (12)$$

A priori, the pointlike limit hence ignores a substantial amount of momentum-dependent information.² Most importantly, since bound-state formation is encoded in the momentum structure of correlation functions (e.g. as s -channel poles in Minkowski space), we cannot expect to obtain reliable information about the mass spectrum of the system. Moreover, the formation of a condensate goes along with a singularity in the fermionic four-point function, such that the fermionic pointlike description cannot access the symmetry-broken regime.

In turn, this implies that the pointlike limit can only be used to study the system within the symmetric regime. In fact, it is adequate to address the large- N_f limit which is expected to lie in the symmetric phase. By lowering the flavor number N_f , we can therefore study the approach to the symmetry-broken phase of the theory, as symmetry-breaking inevitably goes along with a breakdown of the pointlike description. In this manner, we can determine a conformal-critical flavor number $N_{f,\text{cr}}^{\text{qc}}$ below which the pointlike description breaks down, possibly indicating condensate and bound-state formation. In the case that the approach to $N_{f,\text{cr}}^{\text{qc}}$ from above exhibits a clear signature for condensation in a particular channel, the conformal-critical flavor number can agree with a specific critical flavor number $N_{f,\text{cr}}$ below which the system is in a particular symmetry-broken phase. This reasoning has been used in [54–56] to determine the many-flavor phase diagram of QCD.

However, because of the diversity of possible symmetry-breaking patterns as discussed below, the meaning of $N_{f,\text{cr}}^{\text{qc}}$ in QED₃ is less obvious. In fact, our results indicate that there may exist more than one critical flavor number corresponding to different symmetry-broken phases. The

²The functional renormalization group approach used below actually reinstates part of the momentum-dependent information in an effective manner.

conformal-critical flavor number $N_{f,cr}^{qc}$, which we aim to estimate in the present work, provides an upper bound on the potentially existing critical flavor numbers for all kinds of broken phases.

III. SYMMETRY-BREAKING PATTERNS

Let us discuss the various symmetry-breaking patterns that can arise if the fermion self-interactions become critical. Symmetry breaking can give rise to two fundamentally different fermion mass terms: $im\bar{\psi}\psi$ and $i\bar{m}\bar{\psi}\gamma_{45}\psi$. Further fermion bilinears involving γ_4 and γ_5 are $U(2N_f)$ equivalent to these mass terms.

The relation between fermion mass generation and symmetry breaking becomes transparent by means of a Hubbard-Stratonovich transformation [57,58]. This partial bosonization allows us to treat composites of two fermions in terms of effective bosons, schematically, $\phi \sim \bar{\psi}\psi$. More formally, such a transformation allows us to trade in the four-fermion interaction term for a corresponding term bilinear in bosonic fields and a Yukawa-type interaction term on the level of the path integral:

$$\bar{g}_O(\bar{\psi}\mathcal{O}\psi)^2 \longrightarrow \bar{g}_O^{-1}\phi_O^2 + \bar{\psi}\bar{h}_O\phi_O\psi, \quad (13)$$

where the Yukawa-type coupling \bar{h}_O can possibly be flavor- or Dirac-matrix valued. The quantum numbers and transformation properties of the new bosonic field ϕ_O depend on the exact definition of the four-fermion interaction associated with the operator \mathcal{O} . The Yukawa coupling is normalized such that the four-fermion coupling is reproduced upon integrating out the bosonic field.

From Eq. (13), we deduce that the four-fermion couplings are inversely proportional to the mass term $\sim\phi_O^2$ of the bosonic field. Upon fluctuations, we expect that a full Ginzburg-Landau-type effective potential is generated for the boson field. Therefore, a singularity of the pointlike fermionic coupling goes along with the effective potential developing a nontrivial minimum. If so, the expectation value of ϕ_O serves as an order parameter for symmetry breaking. Vice versa, if we observe a divergence of the fermionic self-interactions at a finite RG scale k_{SB} in the purely fermionic language, this serves as an indication for the possible onset of spontaneous symmetry breaking.

Whereas Fierz completeness can be fully preserved by choosing a suitable basis in the purely fermionic language, simple approximations on the partially bosonized side can actually violate this property. For instance, in mean-field approximations this is known as the ‘‘Fierz ambiguity’’ or ‘‘mean-field ambiguity’’ [59], the resolution of which requires dynamical bosonization techniques on the bosonic side [60–62].

In the present work, we anyway study the system by approaching the phase boundary from the symmetric phase, hence the quantitative details of bosonization are not important for our purpose. In order to get a first picture

of possible symmetry-breaking patterns, let us take a closer look at the partially bosonized version of Eq. (10) that uses the $(V)^2$ and $(S)^2$ channels, which are considered to be the relevant channels also in the Thirring model [62]. Using the irreducible representation in terms of two-component fermions χ , see Appendix A, we get for the vector channel

$$-\frac{\bar{g}_V}{2N_f}(V)^2 \rightarrow \frac{1}{2}\bar{m}_V^2 V_\mu V_\mu - \bar{h}_V V_\mu \bar{\chi}^i \sigma_\mu \chi^i, \quad i = 1, \dots, 2N_f, \quad (14)$$

where V_μ denotes a real vector boson, and the $(S)^2$ channel yields

$$\frac{\bar{g}_\phi}{4N_f}(S)^2 \rightarrow \frac{1}{2}\bar{m}_\phi^2 \phi^{ij} \phi^{ji} + i\bar{h}_\phi \bar{\chi}^i \phi^{ij} \chi^j, \quad (15)$$

where $\phi^\dagger = \phi$ denotes a scalar field represented by a Hermitian $2N_f \times 2N_f$ matrix. The equivalence with the fermionic action holds also on the path integral level, if the bare couplings satisfy the constraint

$$\frac{\bar{h}_\phi^2}{2\bar{m}_\phi^2} = \frac{\bar{g}_\phi}{2N_f}, \quad \frac{\bar{h}_V^2}{2\bar{m}_V^2} = \frac{\bar{g}_V}{2N_f}. \quad (16)$$

Whereas the vector field V_μ is invariant under $U(2N_f)$ transformations, the scalar field transforms according to the bifundamental representation. Different symmetry-breaking patterns arise depending on which bosonic field component eventually develops a finite vacuum expectation value. For instance, if ϕ^{ij} acquires an expectation value $\sim\delta^{ij}$, a fermion mass term $\sim i\bar{m}\bar{\psi}^a\gamma_{45}\psi^a$ is generated. As is obvious from the form of the expectation value, this mass term does not break the $U(2N_f)$ symmetry. It breaks parity and time-reversal symmetry [46]. By contrast, an expectation value of the form

$$\phi^{ij} \sim \begin{pmatrix} 1 & 0 \\ 0 & -1 \end{pmatrix} \quad (17)$$

gives rise to a mass term $im(\bar{\chi}^a\chi^a - \bar{\chi}^{a+N_f}\chi^{a+N_f}) = im\bar{\psi}^a\psi^a$ which corresponds to a symmetry-breaking pattern of the form

$$U(2N_f) \rightarrow U(N_f) \otimes U(N_f). \quad (18)$$

This is the pattern expected to occur for small flavor numbers in QED_3 . For $N_f > 2$, more breaking patterns arising from the scalar sector are in principle conceivable, but have not been considered in the literature so far and will also be ignored in this work.

Another option is that the vector field V_μ develops an expectation value. This would leave the $U(2N_f)$ flavor symmetry intact, but would break Lorentz invariance. Breaking patterns of this type have already been considered during the heyday of the NJL model and the development

of the Higgs mechanism [63–65]. For instance, if the expectation value of V_μ was timelike, the corresponding Goldstone bosons may resemble in some aspects a photon field in temporal gauge. In the present case of QED₃, these Goldstone bosons could mix with the photon. In addition, a massive bosonic excitation and Lorentz violating features in correlation functions could be expected to occur. However, the number of nonperturbative studies of this symmetry breaking scenario and the nature of the transition is limited; see, e.g., [66,67].

IV. RENORMALIZATION GROUP FLOW OF QED₃

The preceding sections already anticipated an RG viewpoint on the model. In fact, our quantitative analysis will be based on the functional RG formulated in terms of the Wetterich equation [68] which is a flow equation for the coarse-grained quantum effective action Γ_k :

$$\partial_t \Gamma_k = \frac{1}{2} \text{STr}[(\partial_t R_k) \cdot [\Gamma_k^{(2)} + R_k]^{-1}]. \quad (19)$$

Here, $\Gamma_k^{(2)}$ is the second functional derivative of Γ_k with respect to the fields, $t = \ln(k/\Lambda)$, and k is a flowing IR cutoff scale which is used to set up the RG flow of the quantum effective action. The regularization is implemented with the aid of the regulator function R_k specifying the details of the Wilsonian momentum shell integrations. In the long-range limit, $k \rightarrow 0$, R_k also vanishes such that all quantum fluctuations have been integrated out. The initial condition of the RG flow is determined by the classical action S in the limit $k \rightarrow \Lambda$: $\Gamma_{k \rightarrow \Lambda \rightarrow \infty} \rightarrow S$. In an exact solution to Eq. (19), the results for physical observables to be read off for $k \rightarrow 0$ should not depend on our specific choice for the regularization scheme, i.e., the function R_k in our case. In this work, we exploit a variation of the scheme to test the predictive power of our approximations; see Sec. VI.

Solving the Wetterich equation yields an RG trajectory in theory space, i.e., the space of all action functionals parametrized for instance by all possible field operators compatible with the symmetries of the theory. In the present work, we confine ourselves to an investigation of the RG flow within a hypersurface of theory space, parametrized by the *Ansatz*

$$\begin{aligned} \Gamma_k[\bar{\psi}, \psi, A] = & \int d^3x \left\{ \bar{\psi} (iZ_\psi \not{\partial} + Z_{\bar{\psi}A\psi} \bar{e}A) \psi \right. \\ & + \frac{1}{2} A_\mu Z_A (-\partial^2) \delta_{\mu\nu} + \partial_\mu \partial_\nu A_\nu \\ & + \frac{1}{2\xi} A_\mu Z_\xi \partial_\mu \partial_\nu A_\nu \\ & \left. + \frac{\bar{g}}{2N_f} (\bar{\psi} \gamma_{45} \psi)^2 + \frac{\bar{g}}{2N_f} (\bar{\psi} \gamma_\mu \psi)^2 \right\}, \quad (20) \end{aligned}$$

where the couplings \bar{g} , \bar{g} , the wave-function renormalizations Z_ψ , Z_A , and the vertex renormalization $Z_{\bar{\psi}A\psi}$, governing the renormalization of \bar{e} , are assumed to be functions of the RG scale k . As discussed above, we consider the four-fermion couplings \bar{g} and \bar{g} in the pointlike limit. In addition, also the coupling $Z_{\bar{\psi}A\psi} \bar{e}$, parametrizing the photon-electron vertex, and the fermionic wave-function renormalization Z_ψ will be considered in the zero-momentum limit. In fact, as the flow equation is local in momentum space, receiving its dominant contributions from momenta $p \simeq k$ for a given scale k , the k dependence of all these couplings can be viewed as an effective momentum dependence of the corresponding vertices and propagators; see also our discussion below.

Within the functional RG approach, the restriction to the pointlike limit is therefore less severe as it may seem: only highly asymmetric momentum dependencies of the vertices are neglected, whereas an overall momentum dependence is effectively parametrized by the k dependence of the couplings.

The situation is slightly but decisively different for the photon wave-function renormalization, which we *a priori* consider to be a function of momentum $Z_A = Z_A(p^2)$. While all qualitative features could still be extracted from the zero-momentum limit, the quantitative description of QED₃ depends rather strongly on the precise form of the momentum dependence of the photon propagator. The reason for this is the qualitative change of the momentum dependence of the polarization tensor $\Pi_{\mu\nu}$,

$$\Pi_{\mu\nu}(p) = (p^2 \delta_{\mu\nu} - p^\mu p^\nu) \Pi(p), \quad (21)$$

across the scale set by the dimensionful QED coupling \bar{e}^2 in three dimensions.³ For instance, in the large- N_f limit, the dressing function of the polarization tensor is known to behave as [78]

$$\Pi(p) \sim \frac{1}{p}, \quad (22)$$

which can have a rather strong effect on the photon wave-function renormalization Z_A ,

$$Z_A(p) = 1 + \Pi(p). \quad (23)$$

We need $Z_A(p^2)$ mainly in order to extract the running of the gauge coupling. Since the momentum dependence of $Z_A(p^2)$ is expected to be sensitive to the value of the gauge

³This is a peculiarity of three-dimensional theories and occurs generically for bosonic propagators dressed by fermion loops; see, e.g., Ref. [69] for further examples. By contrast, no such severe momentum dependence is known in four-dimensional theories: In studies of QED₄ and QCD₄, for example, RG flows using the background-field method [70–72] to compute Z_A have been quite successful; see, e.g., Refs. [56,73–77].

coupling, it appears quantitatively mandatory to resolve the momentum dependence of $Z_A(p^2)$ in QED₃ as accurately as possible.

In addition to the kinetic term of the photon, the gauge sector also comes with a gauge-fixing term with gauge parameter ξ and a corresponding wave-function renormalization Z_ξ . In the present work, we work in the Landau gauge $\xi \rightarrow 0$ which is known to be a fixed point of the RG flow [79–82]. This suggests to choose $Z_\xi = Z_A$ for simplicity.

With these prerequisites, it is in principle straightforward to derive the flow of general action functionals spanned by the *Ansatz* (20). In order to make proper contact with QED₃, we have to provide initial conditions for the flow parameters in Eq. (20). With regard to the classical action Eq. (1), these initial conditions are given at the microscopic UV scale Λ by

$$\begin{aligned} Z_\psi|_{\Lambda \rightarrow \infty} &\rightarrow 1, & Z_A|_{\Lambda \rightarrow \infty} &\rightarrow 1, & Z_{\bar{\psi}A\psi}|_{\Lambda \rightarrow \infty} &\rightarrow 1, \\ \bar{e}^2|_{\Lambda \rightarrow \infty} &> 0, & \bar{g}|_{\Lambda \rightarrow \infty} &\rightarrow 0, & \bar{\bar{g}}|_{\Lambda \rightarrow \infty} &\rightarrow 0. \end{aligned} \quad (24)$$

Note that in particular the four-fermion self-interactions are not considered to be independent parameters. If they appear in the RG flow, they are solely generated by quantum fluctuations.

The RG flows for the couplings can conveniently be formulated for the dimensionless renormalized couplings. For the fermionic interactions, these are given by

$$\tilde{g} = Z_\psi^{-2} k \bar{g} \quad \text{and} \quad g = Z_\psi^{-2} k \bar{\bar{g}}. \quad (25)$$

The running of the fermionic wave-function renormalization in turn can be parametrized in terms of the fermionic anomalous dimension

$$\eta_\psi = -\partial_t \ln Z_\psi. \quad (26)$$

The calculation of the corresponding fermionic flows is straightforward with standard techniques, see Ref. [83], and the results will be summarized below.

The RG flow of the gauge sector requires a more careful discussion. The corresponding definition of the dimensionless gauge coupling is

$$e^2 = \frac{\bar{e}^2 Z_{\bar{\psi}A\psi}^2}{Z_A Z_\psi^2 k}. \quad (27)$$

In ordinary perturbation theory, the Ward identity for the photon-electron vertex enforces $Z_{\bar{\psi}A\psi} = Z_\psi$ to hold at each order in a coupling expansion; see, e.g. [84]. In the Wetterich formulation of the functional RG, the regulator, being introduced as a momentum-dependent mass term, also contributes to the breaking of the gauge symmetry similar to the gauge-fixing procedure. This also affects the Ward identities which are accordingly modified by

regulator-dependent terms [73,74,77,79,81,85–88]. For our case, these terms can be worked out explicitly along the lines of [76,89], yielding the modified relation

$$Z_{\bar{\psi}A\psi} = Z_\psi (1 - C_g g - C_{\bar{g}} \tilde{g}), \quad (28)$$

where C_g and $C_{\bar{g}}$ are constants depending on the number of fermion flavors as well as the regularization scheme.

At this point, let us schematically define the photon anomalous dimension analogously to Eq. (26) as $\eta_A = -\partial_t \ln Z_A$ (a more precise definition also accounting for the momentum dependence of Z_A will be given below). Then, the flow equation for the gauge coupling (27) reads

$$\partial_t e^2 = (\eta_A - 1) e^2 - 2e^2 \frac{(C_g(\partial_t g) + C_{\bar{g}}(\partial_t \tilde{g}))}{(1 - C_g g - C_{\bar{g}} \tilde{g})}. \quad (29)$$

In addition to the first term expected from perturbation theory, we encounter additional terms proportional to the flows of the fermion couplings which diagrammatically correspond to a resummation of a large class of diagrams. Below, we will investigate the approach to possible phase transitions as a function of N_f by means of a fixed-point analysis. As fixed points are defined as points in theory space where the RG flow vanishes, i.e., $\partial_t g = \partial_t \tilde{g} = 0$, the additional terms in Eq. (29) vanish identically at the fermionic fixed points and thus are irrelevant for the determination of the fixed point of the full system. For our fixed-point analysis presented below, these additional terms can therefore be ignored.

Finally, we have to give a precise definition of the photon anomalous dimension in order to complete our set of flow equations for our truncation. The evaluation of the photon polarization tensor, corresponding to the diagram in Fig. 1, yields a fully momentum-dependent wave-function renormalization $Z_A(p^2)$. Since the integrand of the momentum trace in the flow equation by construction is peaked for loop-momenta q near the regulator scale, $q^2 \simeq k^2$, it is crucial to obtain a reliable estimate of the gauge coupling

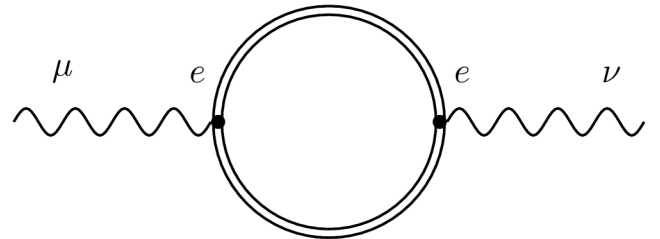


FIG. 1. 1PI diagram contributing to the vacuum polarization tensor $\Pi_{\mu\nu}$: the double lines represent (full) scale-dependent regularized fermion propagators. The flow of the photon wave-function renormalization is driven by the scale derivative of this diagram with respect to the regulator.

that parametrizes the photon-fermion interaction strength of the modes interacting at momentum transfer of the order of the scale k . As the running of the gauge coupling is dominated by the photon anomalous dimension (at least near fermionic fixed points), we define η_A with the aid of the scale derivative of $Z_A(p^2)$ at a momentum scale p^2 evaluated near k^2 . To be more specific, we define

$$\eta_A = -\partial_t \ln Z_A(p^2 = \zeta^2 k^2) \quad (30)$$

where ζ serves as a control parameter that can be used to estimate the dependence of our final results on the details of the definition of η_A and thus on the definition of the gauge coupling. The parameter ζ fixes the momentum scale p serving as the (re)normalization point of the photon field amplitude relative to the Wilsonian momentum shell k . Large values of $\zeta \gg 1$ therefore appear to be artificial, since the physically relevant momenta would then lie far beyond the Wilsonian momentum shell. As a consequence, we expect η_A to be a decreasing function of ζ for large ζ for purely kinematical reasons. The natural range of physically relevant ζ values hence is $0 \leq \zeta \lesssim 1$, with $\zeta \rightarrow 0$ corresponding to the pointlike limit. For a more adapted resolution of nontrivial momentum dependencies of $Z_A(p^2)$, the choice $\zeta = 1$ appears *a priori* preferable.

In the determination of $Z_A(p^2)$ via the polarization tensor, another subtlety is hidden: the standard Ward identity for the polarization tensor $p_\mu \Pi(p)_{\mu\nu} = 0$ is also affected by the presence of the regulator, yielding a nonzero regulator-dependent term on the right-hand side that vanishes in the limit $k \rightarrow 0$. This is a known peculiarity of the present Wilsonian type of RG flow; see, e.g., Refs. [73,74,77,87,88,90–92] for a more detailed discussion of this issue. In order to avoid a contamination of our gauge coupling definition with these artificial regulator-dependent terms, we subtract the $p \rightarrow 0$ limit of $\Pi_{\mu\nu}$ for finite k in the determination of $Z_A(p^2)$. This guarantees that the information entering the anomalous dimension η_A is not contaminated by contributions that arise in the RG flow only in order to satisfy the regulator-dependent constraint on the (unphysical) longitudinal modes. The technical details of the construction of η_A are summarized in Appendix C. In any case, the result for η_A has a comparatively simple form,

$$\eta_A = 8v_3 N_f e^2 \mathcal{L}_1^{(F)}(\eta_\psi; \zeta), \quad (31)$$

where $v_3 = 1/(8\pi)^2$, and $\mathcal{L}_1^{(F)}$ denotes a threshold function that corresponds to the regularized one-particle irreducible (1PI) Feynman diagram shown in Fig. 1. It depends on the choice of the regulator, thus encoding the RG-scheme dependence, and also on the control parameter ζ introduced above. The dependence on the fermion anomalous

dimension η_ψ signals the ‘‘RG improvement’’ inherent in the functional RG. The explicit integral representation of $\mathcal{L}_1^{(F)}(\eta_\psi; \zeta)$ can be found in Eq. (C6).

For the fermion anomalous dimension we find

$$\eta_\psi = \frac{16}{3} v_3 e^2 (m_{2,1}^{(F,B)}(\eta_\psi, \eta_A) - \tilde{m}_{1,1}^{(F,B)}(\eta_\psi, \eta_A)), \quad (32)$$

with the regulator-dependent threshold functions $m_{2,1}^{(F,B)}$ and $\tilde{m}_{1,1}^{(F,B)}$, as defined, e.g., in Refs. [83,93,94]. As the threshold functions are linear in the anomalous dimensions, Eqs. (31) and (32) can unambiguously be solved for η_ψ and η_A as functions of the gauge coupling.

The RG β functions for the fermion sector read

$$\begin{aligned} \partial_t \tilde{g} &= (1 + 2\eta_\psi) \tilde{g} - 8v_3 \left(\frac{2N_f - 1}{N_f} \tilde{g}^2 - \frac{3}{N_f} \tilde{g}g - \frac{2}{N_f} g^2 \right) l_1^{(F)} \\ &\quad - 8v_3 (2\tilde{g}e^2 + 4ge^2) l_{1,1}^{(F,B)} + 16v_3 N_f e^4 l_{2,1}^{(F,B)}, \end{aligned} \quad (33)$$

$$\begin{aligned} \partial_t g &= g(1 + 2\eta_\psi) + 8v_3 \left(\frac{1}{N_f} \tilde{g}g + \frac{2N_f + 1}{3N_f} g^2 \right) l_1^{(F)} \\ &\quad - \frac{8}{3} v_3 (4\tilde{g}e^2 - 2ge^2) l_{1,1}^{(F,B)}, \end{aligned} \quad (34)$$

where the threshold functions l again carry the regulator dependence and depend linearly on η_ψ via $l_1^{(F)}$. For the evaluation of the photon exchange diagrams, we neglect the full momentum dependence of the photon propagator, but take the photon field renormalization at the renormalization point $Z_A(p^2) = Z_A(\zeta^2 k^2)$ into account. Hence, the threshold functions $l_{1,1}^{(F,B)}$ and $l_{2,1}^{(F,B)}$ depend also on η_A . For the so-called sharp cutoff, Eqs. (33)–(34) are equivalent to the results reported in Ref. [30]. In the limit of large flavor number N_f , they also reduce to the large- N_f flow equations found previously within the conventional Wilsonian RG approach [29]. We would like to add that the sharp-cutoff regulator has to be handled with some care. Whereas this type of regulator can be used to compute the flow equations for the pointlike four-fermion couplings without any difficulty, the computation of the flow equations for the wave-function renormalizations suffers from ambiguities which can be traced back to the fact that there is no unique definition for this regulator; see Appendix B. Since the photon wave-function renormalization plays a prominent role in our study of the many-flavor phase structure, we refrain from using this regulator in the following. Instead, we only consider a smeared-out version of this regulator which is free of these difficulties.⁴ For the latter we have

⁴This amounts to using a finite value for the parameter b in our definition of the sharp-cutoff regulator; see Eq. (B6).

found that it yields results for the phase structure that are in accordance with those reported in Sec. VI below.

For vanishing gauge coupling $e^2 = 0$, we observe that the fermionic β functions (33) and (34) vanish identically if g, \tilde{g} are zero at a particular scale [as, e.g., required by the initial conditions (24)]. This obvious fixed point of the flow corresponds to the noninteracting Gaussian fixed point of the theory. For $e^2 \neq 0$, the point of vanishing fermionic couplings is no longer a fixed point due to the last term $\sim e^4$ in Eq. (33).

Finally, the flow of the gauge coupling is given by Eq. (29) upon insertion of the anomalous dimension η_A and the fermionic flows. Near fixed points of the fermionic flow, where $\partial_t g, \partial_t \tilde{g} \approx 0$, the β function of the gauge coupling simplifies to

$$\beta_{e^2} \equiv \partial_t e^2 = (\eta_A - 1)e^2. \quad (35)$$

For the fixed-point analysis carried out in the present work, we consider this simplified flow.

We close this section with a few comments on the reliability of the approximations involved in our truncation. In our numerical studies, we indeed find that $|\eta_\psi| \lesssim 1$ in the symmetric large- N_f regime where the RG flow is governed by the presence of a fixed point; see also our discussion in the subsequent section. This is a strong support for our implicit assertion that momentum dependencies in the fermion sector are less important, such that higher derivative terms of fermionic operators can safely be dropped in this regime. Moreover, it is worthwhile to point out that in the pointlike limit the RG flow of a Fierz-complete set of four-fermion couplings is completely decoupled from the RG flow of fermionic n -point functions of higher order. In particular, 8-fermion interactions do not contribute to the flow of the four-fermion interactions in this limit. This observation corroborates the truncation on the four-fermion level. Further tests of the truncation—particularly of the gauge sector—will actively be pursued in the following sections by studying the amount of artificial regularization-scheme dependence of observables.

V. FIXED-POINT ANALYSIS

The RG fixed-point structure of a theory is intimately related to the phase diagram. Fixed points are defined as common zeros of all β functions, in our case by the requirement

$$\partial_t e^2|_{e_*^2, g_*, \tilde{g}_*} = \partial_t g|_{e_*^2, g_*, \tilde{g}_*} = \partial_t \tilde{g}|_{e_*^2, g_*, \tilde{g}_*} = 0, \quad (36)$$

where e_*^2, g_*, \tilde{g}_* denote the values of the dimensionless couplings at the fixed point. Whereas the fixed-point values themselves are nonuniversal, i.e., depend on the choice of the regularization scheme, the critical exponents as well as the anomalous dimensions $\eta_{\psi,*}$ and $\eta_{A,*}$ at a fixed point are universal. Summarizing all couplings in $\mathbf{G} = (e^2, g, \tilde{g})$,

the critical exponents θ_I are defined in terms of (minus) the eigenvalues of the stability matrix B_i^j ,

$$\partial_t G_i = \beta_i(\mathbf{G}), \quad B_i^j = \left. \frac{\partial \beta_i}{\partial G_j} \right|_{\mathbf{G}=\mathbf{G}_*}, \quad (37)$$

with $-\theta_I$ labeling the eigenvalues of B_i^j , and I running from 1 to the number of couplings considered ($I = 1, 2, 3$ in our case). For instance, at the Gaussian fixed point, $\mathbf{G} = 0$, we have $\theta_I = \{+1, -1, -1\}$, with the positive exponent $+1$ related to the RG relevant gauge coupling. The negative exponents -1 correspond to the RG irrelevant fermionic couplings in QED₃. At the Gaussian fixed point, the critical exponents simply correspond to the power-counting dimension of the couplings.

In order to illustrate the fixed-point structure of the theory, let us start with the flow of the gauge coupling. Assuming that the fixed-point conditions for the fermion couplings are satisfied, we can use Eq. (35). In addition to the Gaussian fixed point, a non-Gaussian, i.e., interacting, fixed-point exists for

$$\eta_{A,*} = 1, \quad e_*^2 = \frac{1}{8v_3 N_f \mathcal{L}_1^{(F)}(\eta_{\psi,*}; \zeta)}, \quad (38)$$

where the threshold function $\mathcal{L}_1^{(F)}$ with η_ψ evaluated at the IR fixed point is a regulator-dependent but real-valued positive number.⁵ The crucial observation is that the value of the fixed point scales with the flavor number N_f as $e_*^2 \sim 1/N_f$.

Starting the RG flow near the Gaussian fixed point at $e^2 \ll 1$, the β function $\partial_t e^2$ is negative, implying that the coupling is asymptotically free towards the UV and increases towards the IR. Hence, the gauge coupling is expected to approach the non-Gaussian fixed point in the long-range limit; see Fig. 2. As long as no fermion-mass generating phase transition occurs in which case the dynamics of the theory would be governed by a different sector of the theory, the whole system remains massless and the IR fixed point [Eq. (38)] is reached asymptotically at small momentum scales. In that case, the theory is quasiconformal, i.e., near conformal in the UV near the Gaussian fixed point as well as near conformal in the IR near the non-Gaussian fixed point. The two near-conformal regimes are smoothly connected by a crossover occurring at momentum scales near the scale approximately set by the bare coupling \bar{e}^2 . Note that the maximum coupling strength

⁵Negative values could only occur for very large $\eta_{\psi,*}$ which would indicate the breakdown of our truncation anyway. For all flows studied in this work, η_ψ generically remains rather small, $|\eta_\psi| \lesssim 1$, provided that the dynamics is governed by a fixed point. If, on the other hand, the IR fixed point of the gauge coupling is destabilized by, e.g., spontaneous (chiral) symmetry breaking, then η_ψ may grow rapidly as well. However, a detailed analysis of this scenario is beyond the scope of our present work.

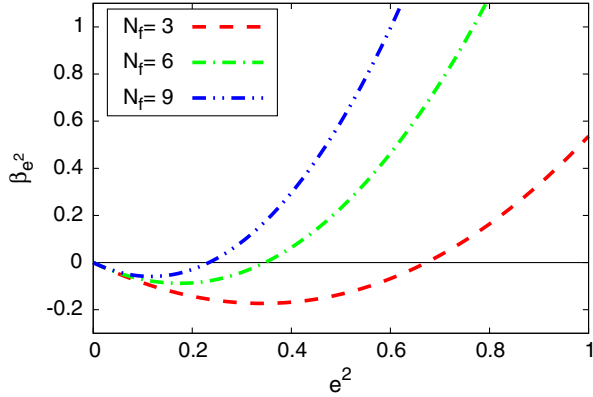


FIG. 2 (color online). β_{e^2} function for three different values of N_f as obtained from the linear regulator evaluated for $\zeta = 1$.

of the dimensionless coupling is set by the IR fixed-point value; see Eq. (38). In particular, the maximum coupling strength is smaller for larger flavor numbers.

Let us now turn to the fermionic sector with the corresponding flows given in Eqs. (33) and (34), treating the gauge coupling as an external parameter for the moment. As the fixed-point conditions for g and \tilde{g} [Eq. (36)] correspond to two coupled quadratic equations, we generically expect up to four distinct fixed-point solutions. Provided that the gauge coupling is sufficiently small, we find four distinct real solutions which thus represent candidates for physically relevant fixed points. For finite $e^2 > 0$, these points in coupling space are no longer fixed points of the total system, as their positions change with the gauge coupling e^2 . In a slight abuse of language, we still call them fixed points, as for a given value of e^2 they govern the flow in the fermionic sector. In the limit $e^2 \rightarrow 0$, one of the four fixed points is continuously connected to the (true) Gaussian fixed point at $\mathbf{G} = 0$. For small but finite e^2 , this fixed point is slightly shifted to nonzero couplings \tilde{g}_*, g_* but continues to have two RG irrelevant directions. This fixed point, named \mathcal{O} in Fig. 3, is thus IR attractive in the (\tilde{g}, g) plane. Two further fixed points \mathcal{A} and \mathcal{C} have one IR attractive (RG irrelevant) and one IR repulsive (RG relevant) direction, and the fixed point \mathcal{B} exhibits two IR repulsive directions; see Fig. 3.

For vanishing gauge coupling, $e^2 = 0$, the Gaussian fixed point \mathcal{O} describes a free theory of noninteracting fermions. The fixed point \mathcal{C} has been extensively studied in [45,46,62]. It can be associated with the asymptotically safe three-dimensional Thirring model. For sufficiently small flavor numbers $N_f < N_{f,\text{cr}}^{\text{Thirring}}$, the fixed point controls a second-order quantum phase transition, separating the massless phase from the phase of chiral symmetry breaking; see, e.g., [95] for a study of the $N_f = 1$ model. In Refs. [46,62], the critical flavor number of the Thirring model has been estimated as $N_{f,\text{cr}}^{\text{Thirring}} \simeq 5.1$. Lattice studies of the Thirring model with a different realization

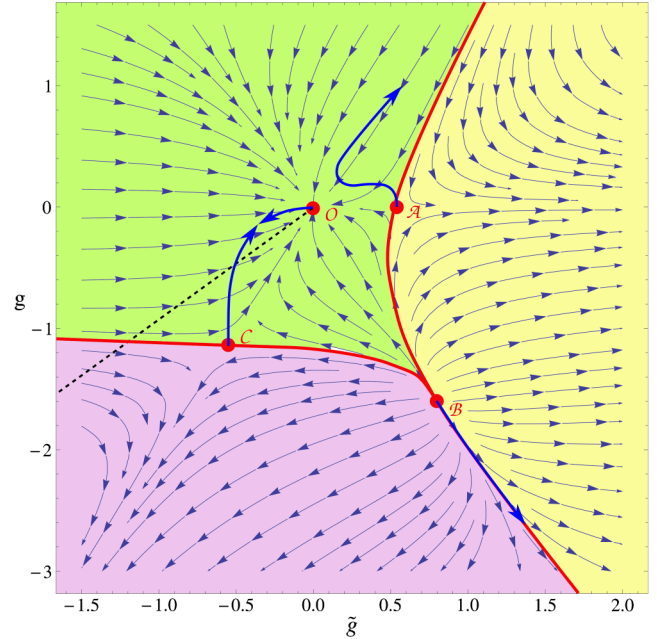


FIG. 3 (color online). RG trajectories in the plane spanned by the four-fermion couplings \tilde{g} and g for $N_f = 4$ and $e^2 = 0$ using the linear regulator. The fixed points are depicted by the red dots, where \mathcal{O} is the IR stable Gaussian fixed point, \mathcal{A} and \mathcal{C} are fixed points with one IR attractive and one IR repulsive direction, and \mathcal{B} is an unstable fixed point with two IR repulsive directions. The thin arrows indicate the RG flow towards the IR regime. The dashed line ($g = \tilde{g}$) corresponds to the chiral channel (where $g_V = 0$ and g_ϕ is nonzero), potentially associated with chiral symmetry breaking; see also Eq. (11). This channel is typically chosen in Fierz-incomplete studies. The blue/bold arrows attached to the four fixed points indicate the shift of the fixed points induced by an increase of the gauge coupling $e^2 > 0$.

of the chiral symmetry using staggered fermions found $N_{f,\text{cr}}^{\text{Thirring}} \simeq 6.6$ [96].⁶

The fixed-point \mathcal{A} corresponds to a variant of the three-dimensional Gross-Neveu model. Different versions of this model exist in $d = 3$, all of which are asymptotically safe because of such a non-Gaussian fixed point [105–107]. This fixed point governs the second-order quantum phase transition of a discrete \mathbb{Z}_2 symmetry (parity symmetry in this case) which is known to occur for any N_f . By contrast, the fixed point \mathcal{B} has less well been studied, but could equivalently give rise to an asymptotically safe fermionic model potentially exhibiting first-order phase transitions to various phases in the IR.

Returning now back to QED₃, the initial conditions (24) put the system into the vicinity of the Gaussian fixed-point \mathcal{O} at the microscopic scale $k \rightarrow \Lambda$, leaving us with one RG

⁶In the literature, estimates for the critical flavor number of the Thirring model span a wide range of values [96–104]. Many of the analytical estimates show a strong similarity to the corresponding QED₃ results.

relevant parameter, namely the gauge coupling, as it should be. Towards the UV, the full system is asymptotically free. Towards the IR, the gauge coupling increases, shifting the Gaussian fixed point \mathcal{O} slightly in the (\tilde{g}, g) plane; see blue/bold arrows in Fig. 3. Since \mathcal{O} remains IR attractive in the fermionic directions, the flow of \tilde{g}, g follows this IR attractive fixed point.

If the gauge coupling approaches a critical value e_{cr}^2 , the fixed points \mathcal{C} and \mathcal{O} annihilate; see Fig. 3. If we increase the gauge coupling even further, then the flow of the four-fermion couplings is no longer bounded by the existence of an IR attractive fixed point. On the contrary, the four-fermion interactions start to grow rapidly and diverge at a finite RG scale k_{SB} , potentially indicating dynamical symmetry breaking, as discussed above.

From the fixed-point analysis itself, we do not gain immediate insight into the exact type of spontaneous symmetry breaking, as this is a result of the full RG flow towards the IR. Nevertheless, the fixed-point analysis provides for a criterion for symmetry breaking to be possible at all: as long as the fixed-point \mathcal{O} exists, being IR attractive for the fermionic couplings, no approach to criticality in the fermion sector can occur. Thus, monitoring the existence of this fixed point as a function of N_f provides first information about the structure of the phase diagram as a function of N_f .

VI. CONFORMAL-CRITICAL FLAVOR NUMBER

From the preceding discussion, we expect the system to be quasiconformal as long as the fixed-point \mathcal{O} in the fermion sector persists and remains IR attractive in the fermionic couplings. The fixed-point \mathcal{O} vanishes if the gauge coupling exceeds a critical coupling strength e_{cr}^2 . In the quasiconformal phase, the IR fixed point e_*^2 as given in Eq. (38) is a measure for the maximum coupling strength. Since e_*^2 is small for large N_f , the quasiconformal phase occurs at large N_f extending to $N_f \rightarrow \infty$. Lowering N_f , the annihilation of the fixed-points \mathcal{O} and \mathcal{C} indicate the boundary of the quasiconformal phase and a possible onset of a different phase. The corresponding value of N_f defines the conformal-critical flavor number $N_{f,\text{cr}}^{\text{qc}}$ which is defined by the criticality condition

$$e_*^2(N_{f,\text{cr}}^{\text{qc}}) \stackrel{!}{=} e_{\text{cr}}^2(N_{f,\text{cr}}^{\text{qc}}). \quad (39)$$

See also Fig. 4. Whereas both e_*^2 and e_{cr}^2 are nonuniversal and depend on the choice of the regularization scheme, the conformal-critical flavor number $N_{f,\text{cr}}^{\text{qc}}$ is expected to be universal.⁷ However, the fact that we consider an

⁷Since $N_{f,\text{cr}}^{\text{qc}}$ presumably is not an integer, its value might depend on the manner, how theories with noninteger flavor numbers are constructed. Nevertheless, the result that systems with integer $N_f > N_{f,\text{cr}}^{\text{qc}}$ have long-range properties substantially different from those with integer $N_f < N_{f,\text{cr}}^{\text{qc}}$ is in principle a universal and observable phenomenon.

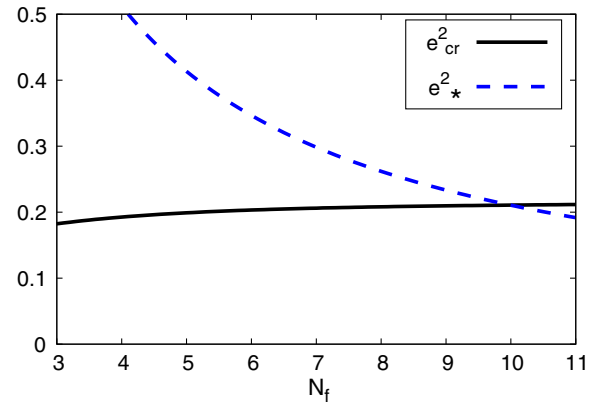


FIG. 4 (color online). The critical value e_{cr}^2 for the gauge coupling and the value e_*^2 of the IR fixed point as a function of N_f as obtained from the linear regulator for $\zeta = 1$. The intersection point of both lines determines the conformal-critical flavor number $N_{f,\text{cr}}^{\text{qc}}$; see Eq. (39). Note that the depicted N_f dependence of e_*^2 has been computed with the aid of Eq. (35). However, the associated IR fixed-point e_*^2 is only approached for $N_f \geq N_{f,\text{cr}}^{\text{qc}}$. For $N_f < N_{f,\text{cr}}^{\text{qc}}$, this fixed point is destabilized due to spontaneous symmetry breaking.

approximation of the exact RG flow implies that also the universality of $N_{f,\text{cr}}^{\text{qc}}$ holds only approximately.

In Table I, we list our results for $N_{f,\text{cr}}^{\text{qc}}$ as obtained from our computations with three different regulator functions; see Appendix B for the definitions of these functions. We also consider two different values of the control parameter ζ which parametrizes the external photon momentum of the vacuum polarization diagram relative to the cutoff scale; cf. Eq. (30). Whereas the choice $\zeta = 1$ appears more adapted to resolve the momentum dependence of the photon wave function, the choice $\zeta = 0$ conforms with the pointlike approximation in the fermion sector. In either case, we obtain the smallest value of $N_{f,\text{cr}}^{\text{qc}}$ for the Callan-Symanzik regulator. Since the latter is equivalent to a mass term $\sim k$ without any momentum dependence, it does not entail a UV suppression and therefore is likely to give rise to stronger truncation artifacts, as is also known from many other RG studies. The two other regulators, the exponential and the linear regulator, cf., Appendix B for details, provide for both a UV and IR regularization and are thus considered as quantitatively more reliable. These two regulators span the range of estimates for $N_{f,\text{cr}}^{\text{qc}}$ of $N_{f,\text{cr}}^{\text{qc}} \simeq 8, \dots, 10$ for $\zeta = 1$ and $N_{f,\text{cr}}^{\text{qc}} \simeq 4, \dots, 5.7$ for $\zeta = 0$ with the largest $N_{f,\text{cr}}^{\text{qc}}$ value arising from the linear regulator, respectively. Intermediate values of ζ yield ranges that interpolate between the $\zeta = 0$ and $\zeta = 1$ cases.⁸ We observe that the variation with respect to the control parameter ζ is even larger than the regulator

⁸Incidentally, a smeared version of the sharp cutoff with smearing parameter $b \simeq 2$ (see Appendix B) yields values for $N_{f,\text{cr}}^{\text{qc}}$ within the ranges spanned by the exponential and the linear regulator.

TABLE I. Conformal-critical flavor number for different regulator functions, Callan-Symanzik regulator (CS), exponential regulator (exp), linear regulator (lin), and for different choices of the control parameter $\zeta = 1$ and $\zeta = 0$.

Regulator	R_{CS}	R_{exp}	R_{lin}
$N_{f,\text{cr}}^{\text{qc}}(\zeta = 1)$	7.5	8.1	10.0
$N_{f,\text{cr}}^{\text{qc}}(\zeta = 0)$	3.7	4.1	5.7

dependence. We interpret this as a signature for the importance of the precise resolution of the momentum dependencies of the correlation functions.

In general, these uncertainties indicate a systematic error to be associated with the employed truncation. For example, the inclusion of the full momentum dependence especially of the photon-propagator and the fermion-photon vertex may be required to determine $N_{f,\text{cr}}^{\text{qc}}$ more precisely. In order to assess the stability of our results for the conformal-critical flavor number, let us discuss the variations of the regulator and the control parameter in more detail: First, the dependence on the regulator is a natural consequence of truncated flows. This dependence can be lifted by identifying “optimized” regularization schemes satisfying *a priori* criteria that can be argued to be closest to the exact results within a given truncation [88,108–110]. The linear regulator is such an optimized regulator for the pointlike limit and with $\zeta = 0$. For $\zeta = 1$, none of our regulators is optimized in a similar sense. Different values of ζ should therefore be considered as different truncations.

According to its definition $\zeta = |p|/k$, the control parameter measures the relation between the incoming photon momentum and the regularization scale of the internal fermion loop of the vacuum polarization diagram; see Fig. 1. For a reconstruction of the full momentum dependence of the photon wave function $Z_A(p^2)$ via the anomalous dimension formula Eq. (30), we hence consider the choice $\zeta = 1$ more reliable. On the other hand, the vacuum polarization diagram is only used to estimate the running coupling, which in turn enters the fermion box diagrams as an estimate for the fermion-photon vertex; see also Fig. 5. This estimate can be afflicted with the following problem: As we evaluate the box diagrams in the pointlike limit, i.e., in the limit of zero external momentum, the vertex enters the flow equations at an asymmetric point, since the internal lines of the diagram carry an in general finite loop momentum. Therefore, potentially asymmetric structures of the vertices are neglected by our approximation. The intrinsic tension between such structures and our estimate for the running coupling could even be amplified by choosing a nonzero ζ .

With this analysis of the regulator and ζ dependence, we can now summarize our estimates for the location of the conformal-critical flavor number $N_{f,\text{cr}}^{\text{qc}}$. From a conservative perspective, we have not been able to find estimates of $N_{f,\text{cr}}^{\text{qc}}$

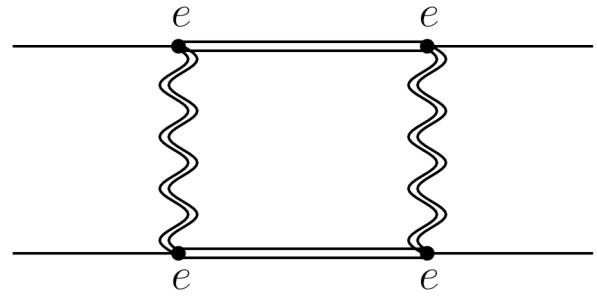


FIG. 5. 1PI diagram contributing to the RG flow of the four-fermion couplings: the double lines represent (full) scale-dependent regularized fermion and photon propagators.

with values smaller than $N_f \approx 3.7$ or larger than $N_f \approx 10.0$ also including extreme regulator choices such as the Callan-Symanzik regulator. We hence conclude $N_{f,\text{cr}}^{\text{qc}}$ to lie within this interval. Excluding the Callan-Symanzik regulator in order to avoid regulator artifacts, our results span a smaller region. The regulator and ζ dependence analysis given above suggest the conformal-critical flavor number of QED₃ to lie in the region

$$N_{f,\text{cr}}^{\text{qc}} \approx 4.1 \dots 10.0. \quad (40)$$

We emphasize, however, that the upper and lower end of this interval should not be viewed as a strict boundary, but may change upon improvements of the approximation. Despite these uncertainties, this estimate represents one of the main results of our study.

VII. FIERZ COMPLETENESS

The above given estimate for the conformal-critical flavor number $N_{f,\text{cr}}^{\text{qc}}$ —though coming with a large uncertainty—appears to include values significantly larger than many results for the critical flavor number for chiral symmetry breaking reviewed in the introduction. While there are many sources that can take a strong influence on the final result (e.g., large finite volume effects in finite-volume studies [41,111]), we emphasize in this work two issues that have not yet received sufficient attention.

First, we have determined the conformal-critical flavor number $N_{f,\text{cr}}^{\text{qc}}$ above which the system is quasiconformal. While this value is likely to mark a region in the many-flavor phase diagram where a crossover or a phase transition is expected to occur, it does not necessarily have to agree with the critical flavor number for the chiral phase transition $N_{f,\text{cr}}^{\zeta}$. As we can only detect the quasiconformal regime with our pointlike approximation, we can only conclude so far that $N_{f,\text{cr}}^{\zeta} \leq N_{f,\text{cr}}^{\text{qc}}$; cf. also next section for a discussion. Hence, there is no immediate disagreement with the literature in this respect.

Second, we have emphasized that our *Ansatz* for the effective action is Fierz complete in the sense that it

includes all pointlike four-fermion interactions compatible with the symmetries of the model. The significance of Fierz completeness for an appropriate description of an approach to criticality is already obvious from our parametrization. The chiral-symmetry breaking channel $(S)^2$ in the Fierz-transformed Lagrangian in Eq. (10) which, when becoming dominant, generates a mass term $\sim im\bar{\psi}^a\psi^a$, is associated with a superposition of both four-fermion channels $\tilde{g}(P)^2$ and $g(V)^2$ used in this work (see dashed line in Fig. 3). Ignoring one of the channels may lead to strong deviations from the Fierz-complete result.

In order to quantify the importance of Fierz completeness, we study the dependence of our result for the conformal-critical flavor number $N_{f,cr}^{qc}$ on a one-parameter family of Fierz-incomplete approximations. To be specific, we first introduce a Fierz-complete reparametrization of the couplings as follows:

$$s_\varphi = g \sin \varphi + \tilde{g} \cos \varphi, \quad (41)$$

$$\tilde{s}_\varphi = g \cos \varphi - \tilde{g} \sin \varphi, \quad (42)$$

where the angle φ parametrizes a family of couplings s_φ , \tilde{s}_φ . From here, we arrive at a Fierz-incomplete set by truncating $\partial_r \tilde{s}_\varphi \equiv 0 \equiv \tilde{s}_\varphi$. The angle φ can now be used to select a specific interaction channel. For example for $\varphi = \pi/4$, we have $\tilde{g} = g$, such that we are left with the chiral channel only; see also Eq. (11) and the dashed line in Fig. 3.

With the φ -dependent Fierz-incomplete approximation at hand, we can now compute the conformal-critical flavor number again. In Fig. 6, we present our results for $N_{f,cr}^{qc}$ as a function of the angle φ for $\zeta = 0$ (upper panel) and $\zeta = 1$ (lower panel). We observe that the predictions for the conformal-critical flavor number strongly vary within this family of Fierz-incomplete approximations. Moreover, we find that a finite range of values for φ exists for which we have $N_{f,cr}^{qc} = 0$. This was to be expected, since for $\pi/2 \lesssim \varphi \lesssim \pi$ we project onto a channel orthogonal to the chiral channel. There is no annihilation of fixed points in this channel for any N_f , since the fixed points \mathcal{A} and \mathcal{B} do not approach the Gaussian fixed-point \mathcal{O} for any value of e^2 ; see blue/bold lines in Fig. 3. This may be interpreted as a consequence of the Vafa-Witten argument [112], prohibiting the spontaneous breaking of parity symmetry in QED₃. As another specific example, let us consider a projection onto the chiral channel corresponding to $\varphi = \pi/4$: here we find $N_{f,cr}^{qc} \approx 5$ even for all studied regulator functions and ζ values. However, this is still significantly different, for instance, from the Fierz-complete result for $\zeta = 1$.

Our analysis clearly demonstrates the necessity of a Fierz-complete treatment as one may significantly overestimate by almost a factor of 2 or underestimate ($N_{f,cr}^{qc} = 0$) the conformal-critical flavor number within a Fierz-incomplete setup; see Fig. 6. This strong ambiguity of $N_{f,cr}^{qc}$ within a

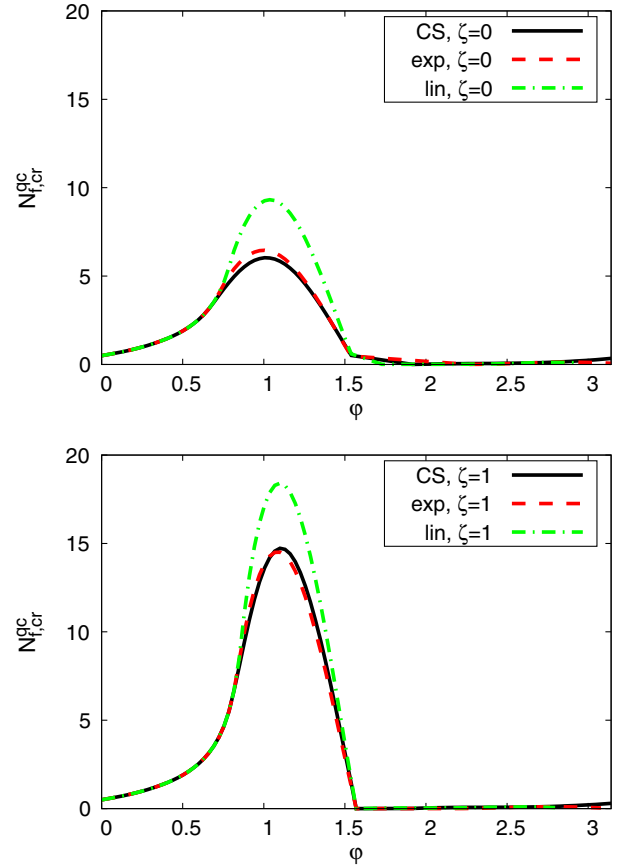


FIG. 6 (color online). Conformal-critical flavor number $N_{f,cr}^{qc}$ as a function of the angle φ parametrizing an artificial Fierz incompleteness for $\zeta = 0$ (top panel) and $\zeta = 1$ (bottom panel).

Fierz-incomplete study represents the second important result of our work. Moreover, any Fierz-incomplete study that is only sensitive to the chiral channel will inevitably identify $N_{f,cr}^{qc}$ with $N_{f,cr}^Z$. In this case, any information about a possibly existing intermediate phase will not be accessible because of Fierz incompleteness.

While Fierz completeness is simple to implement in the present approximation scheme of the exact RG flow, it is less obvious how this issue might affect other methods. Mean-field methods are certainly strongly affected, as the choice of a mean field immediately breaks Fierz completeness [59].

By contrast, lattice simulations are by construction not affected, as no choice of channels is required. Still, our results on Fierz completeness can also be interpreted as a mandate to implement the flavor symmetries exactly. Hence, lattice formulations should be given preference that feature an exact (lattice version of) the $U(2N_f)$ flavor symmetry.

The largest body of literature on chiral-symmetry breaking in QED₃ relies on solutions of Dyson-Schwinger equations for the photon and fermion propagators amended with suitable vertex constructions. For the solution of the

equation for the fermion propagator $S_\psi(p)$, an *Ansatz* of the following form is typically used,

$$S_\psi(p)^{-1} = i\not{p}A(p^2) + B(p^2), \quad (43)$$

where $A(p^2)$ is related to the (inverse) wave-function renormalization, and $B(p^2)$ parametrizes the mass function. In particular, $\lim_{p \rightarrow 0} B(p^2) \neq 0$ signals fermion mass generation and chiral symmetry breaking. This *Ansatz* is also commonly and successfully used for investigations of the strong-coupling regime of QCD in $d = 4$. Here, we note that the *Ansatz* (43) does not exhaust all possible terms permitted by the special Dirac structure and flavor symmetry of QED in $d = 3$. As suggested by our results, the inclusion of all terms permitted by the symmetries might be an essential ingredient. On the level of the fermion propagator, a complete *Ansatz* would read

$$S_\psi(p)^{-1} = i\not{p}A(p^2) + B(p^2) + \gamma_{45}C(p^2) + i\not{p}\gamma_{45}D(p^2), \quad (44)$$

involving two further scalar functions C and D . The case of $\lim_{p \rightarrow 0} C(p^2) \neq 0$ would signal the generation of a parity-breaking mass term. However, even in the parity-symmetric phase where $\lim_{p \rightarrow 0} C(p^2) = 0$, the two further functions might develop a nontrivial momentum dependence at intermediate scales, potentially taking influence on the $B(p^2)$ function and thus on the onset of chiral symmetry breaking.

Let us finally emphasize that there certainly is no one-to-one correspondence between our results for Fierz-incomplete approximations and flavor-symmetry-incomplete DSE *Ansätze* of the type of Eq. (43). It may well be that Eq. (43) is perfectly sufficient to obtain quantitatively reliable results. In QED₃ with a Chern-Simons term, which explicitly breaks parity symmetry, the full *Ansatz* (44) is indeed mandatory. This has been studied previously [113–115], suggesting, however, that on the level of the considered approximations the chiral-critical flavor number seems to be less influenced by the functions $C(p^2)$ and $D(p^2)$ in Eq. (44). It should thus be worthwhile to further investigate whether this still holds in “pure” QED₃ without explicit breaking of parity, in particular with an emphasis on an analysis of the IR limit.

VIII. PHASE STRUCTURE

As our truncation based on pointlike fermion interaction channels is not capable of entering the symmetry-broken regime, the scenario developed in this section is founded only on limited information which we can extract from the RG flow in the symmetric regime. With these reservations in mind, we recall that we have identified a conformal-critical flavor number $N_{f,\text{cr}}^{\text{qc}}$ above which we found QED₃ to be in the quasiconformal phase.

So far, we have carefully distinguished between $N_{f,\text{cr}}^{\text{qc}}$ and a possible critical flavor number $N_{f,\text{cr}}^{\text{Z}}$, indicating the onset of a chirally broken phase. From our results, we can primarily conclude that $N_{f,\text{cr}}^{\text{Z}} \leq N_{f,\text{cr}}^{\text{qc}}$. For a first attempt to estimate the possible value of $N_{f,\text{cr}}^{\text{Z}}$ within our approach, let us take a look at the RG flow trajectories in the plane of fermionic couplings for various flavor numbers below $N_{f,\text{cr}}^{\text{qc}}$. For illustrative purposes, we consider the flows obtained with the linear regulator and a control parameter value $\zeta = 1$, which yielded the estimate $N_{f,\text{cr}}^{\text{qc}} \approx 10$. Also, we fix the gauge coupling slightly above the critical value e_{cr}^2 where the fixed-points \mathcal{O} and \mathcal{C} annihilate, $0 < (e^2 - e_{\text{cr}}^2) \ll 1$.

The resulting fermionic flows in the (\tilde{g}, g) plane are shown in Fig. 7 for the case of $N_f = 1$ (left panel) and $N_f = 9$ (right panel). As before, the dashed line ($g = \tilde{g}$) corresponds to the chiral channel (S)², potentially associated with chiral symmetry breaking when becoming dominant. The solid red line marks the direction of the asymptote of the RG trajectories for large \tilde{g}, g . Starting the flow for vanishing fermionic interactions $\tilde{g} = g = 0$, in general both \tilde{g} and g are generated and will approach this asymptote in the course of the RG flow. The slope of the RG asymptote thus determines the relative weight of the different possible channels in the IR. For $N_f = 1$ (left panel of Fig. 7), it is fairly close to the dashed line associated with symmetry breaking in the chiral channel; in fact, for $N_f = 1.75$ (not shown) the RG asymptote would lie exactly on top of the chiral channel. By contrast, the $N_f = 9$ asymptote is closer to the pure vector channel $\sim g(V)^2$. The fact that this asymptote rotates with increasing N_f towards the vector channel is already known from studies of the Thirring model [45,62]. In fact, the depicted flows agree with those of the Thirring model for asymptotically large g and \tilde{g} , as we have kept the gauge coupling at a fixed finite value. For any $N_f < N_{f,\text{cr}}^{\text{qc}}$, the RG asymptote in QED₃ thus coincides with the Thirring-model asymptote within our approximation.

On the basis of our pointlike fermionic truncation it is hard to judge which channel ultimately dominates as a function of N_f . This is because we do not have a metric in theory (coupling) space available that could provide for a quantitative measure of absolute distance from a certain channel. As a tentative measure for the chiral symmetry-breaking region, we have depicted a gray shaded region between the angle bisectrix between the chiral axis and the \tilde{g} axis and the one between the chiral axis and the g axis.

For small N_f such as $N_f = 1$, the asymptote lies inside this region where we expect chiral symmetry-breaking to occur; cf. Fig. 7 (left panel). For larger N_f such as $N_f = 9$, the asymptote lies outside this region; cf. Fig. 7 (right panel). Taking this rough measure seriously, we find that the asymptote of the four-fermion flows lies within this suspected domain of attraction of the chiral channel for $1 \lesssim N_f \lesssim 4$. As a rough estimate, this suggests that one

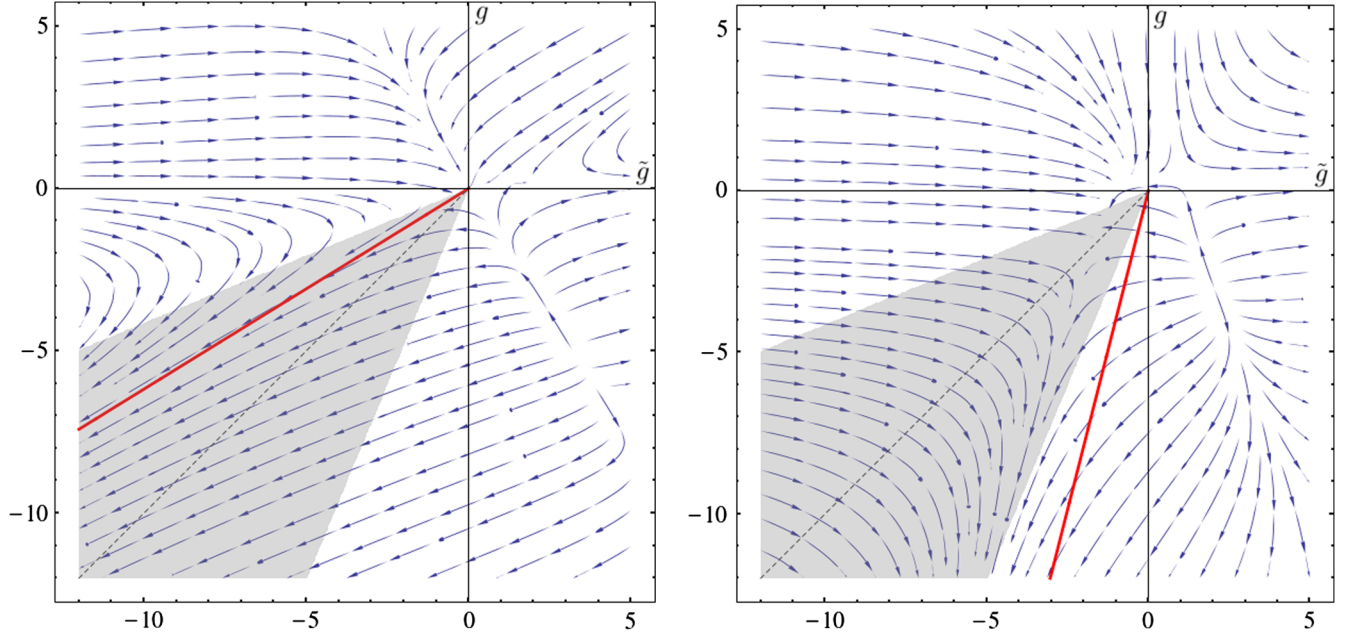


FIG. 7 (color online). RG flow of the four-fermion interactions in the plane spanned by the couplings \tilde{g} and g for $0 < (e^2 - e_{\text{cr}}^2) \ll 1$ and $N_f = 1$ (left panel) and $N_f = 9$ (right panel), as obtained from the linear regulator function with $\zeta = 1$. Recall that $N_{f,\text{cr}} = 10.0$ in this case. The dashed line corresponds to the chiral channel ($\tilde{g} = g$). The solid red line represents the asymptotes of the RG trajectories. The gray shaded area indicates a tentative measure for the chiral symmetry-breaking region; see main text for details.

identifies the maximal value of N_f , for which the system is inside this region with a dominant chiral channel, with the critical flavor number for chiral-symmetry breaking $N_{f,\text{cr}}^\zeta$. Independent of our choice for the regulator function, we find the estimate $N_{f,\text{cr}}^\zeta \approx 4$, which is in the ballpark of the most advanced DSE studies [28,38,41–43].

For the linear regulator in the pointlike limit $\zeta = 0$ and for all regulators with $\zeta = 1$, we find that the chiral-critical flavor number can in fact be smaller than the conformal-critical flavor number, $N_{f,\text{cr}}^\zeta < N_{f,\text{cr}}^{\text{qc}}$. This leaves us with the interesting conclusion that the many-flavor phase diagram of QED₃ could be more involved than previously anticipated: in addition to the chiral symmetry broken phase for $N_f < N_{f,\text{cr}}^\zeta$ and the quasiconformal phase for $N_f > N_{f,\text{cr}}^{\text{qc}}$ there could be another phase in between for $N_{f,\text{cr}}^\zeta < N_f < N_{f,\text{cr}}^{\text{qc}}$ characterized by different low-energy properties.

At this point, it is instructive to compare our results with those from the 3D Thirring model which shares with QED₃ both its $U(2N_f)$ chiral symmetry as well as the corresponding possible symmetry-breaking patterns. In the Thirring model, defined in terms of the non-Gaussian UV fixed-point \mathcal{C} (for $e^2 = 0$), the long-range chiral properties in the pointlike language are also determined by the competition between the chiral and the vector channel. In [62] the Thirring model was studied in detail using dynamical bosonization techniques that allow one to enter the symmetry-broken regime and give direct access to the order-parameter potentials, condensation phenomena, and massive excitations. The critical flavor number below

which the system is in the chiral symmetry broken phase was determined to be

$$N_{f,\text{cr}}^{\zeta,\text{Thirring}} \approx 5.1, \quad (45)$$

which is similar to our rough estimate for $N_{f,\text{cr}}^\zeta$ for QED₃ given above. In fact the mere quantitative difference between our QED₃ flows and those of the Thirring model within the same approximation in the fermion sector are the gauge-coupling terms in the β functions. As the approach to criticality is primarily indicated by diverging four-fermion interactions, the following scenario is possible: if the gauge contributions to the fermion self-interactions stay subdominant for the approach to criticality, we conjecture that the critical flavor number of QED₃ and the 3D Thirring model are identical.

For this conjecture to hold, the chiral-critical flavor number of the Thirring model must not lie in the quasiconformal regime of QED₃. With our result for the conformal-critical flavor number, $N_{f,\text{cr}}^{\text{qc}} > N_{f,\text{cr}}^{\zeta,\text{Thirring}}$, this criterion appears to be satisfied within our approximation for the linear regulator in the pointlike truncation with $\zeta = 0$ and for all regulators with $\zeta = 1$. Otherwise the QED₃ system could still be trapped by the IR attractive fixed-point \mathcal{O} while the analogous Thirring system would already be in the chirally broken phase, such that the conjecture would fail. Whether the gauge contributions indeed stay subdominant during the approach to criticality is a quantitative question that we cannot resolve within our present simple truncation. For instance, using the simplified β function for the gauge coupling (35), the gauge coupling remains

bounded by its fixed-point value, $e^2 \leq e_*^2$, and the criterion is satisfied. In the more general case, e.g., using Eq. (29), the situation is less clear and requires a full numerical integration of the flow. Most likely a definite answer requires a dynamically bosonized flow. However, even if the gauge contributions do not stay subdominant, it appears plausible that the chiral-critical flavor numbers for QED₃ and the 3D Thirring model would still be similar.

Let us now try to address the new possible phase between $N_{f,\text{cr}}^\chi$ and $N_{f,\text{cr}}^{\text{qc}}$, assuming that $N_{f,\text{cr}}^\chi < N_{f,\text{cr}}^{\text{qc}}$. Again, the Thirring model may provide a guideline: in [62], it was observed that for $N_f > N_{f,\text{cr}}^\chi$, the system not only is dominated by the vector channel, but moreover the mass term of the vector channel m_V^2 approaches zero at a finite scale k . This indicates the possibility of the appearance of a Lorentz symmetry breaking condensate $\langle V_\mu \rangle \neq 0$ for $N_{f,\text{cr}}^\chi < N_f < N_{f,\text{cr}}^{\text{qc}}$, going along with two massless Goldstone bosons and a massive “radial” mode.

These considerations suggest a many-flavor phase diagram of QED₃ as schematically drawn in Fig. 8 with a chirally broken small- N_f phase, possibly a phase with spontaneously broken Lorentz symmetry at intermediate N_f , and a quasiconformal massless phase at large N_f extending to $N_f \rightarrow \infty$. The nature of the phase transitions at $N_{f,\text{cr}}^\chi$ and $N_{f,\text{cr}}^{\text{qc}}$ cannot be determined within our present approximation. For the Thirring model, the dynamically bosonized study revealed that the chiral phase transition at $N_{f,\text{cr}}^\chi$ is of second order [62]. In particular the chirally broken and Lorentz-broken phases do not overlap, but inhibit one another. This suggests the possibility of a second-order phase transition at $N_{f,\text{cr}}^\chi$ also in QED₃, if the gauge coupling does not take too strong of an influence on the approach to criticality.

The nature of the transition at $N_{f,\text{cr}}^{\text{qc}}$ is less clear. On the one hand, the quasiconformal mode vanishes because of the annihilation of fixed points. This is similar to

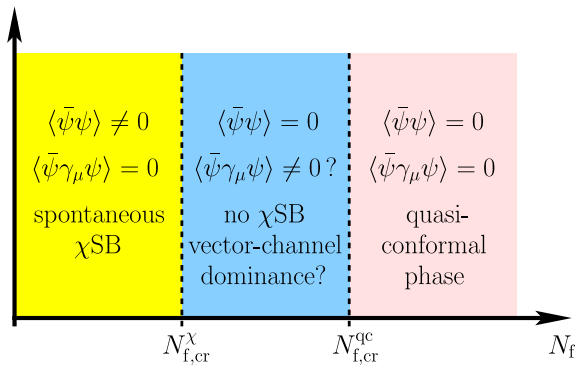


FIG. 8 (color online). Sketch of the conjectured many-flavor phase diagram of QED₃. In addition to the phase governed by spontaneous chiral symmetry breaking (χ SB) for small values of N_f , an intermediate phase driven by the vector-channel may exist, possibly exhibiting (spontaneous) breaking of Lorentz symmetry; see text for a discussion of the transition lines.

Berezinsky-Kosterlitz-Thouless (BKT)-type phase transitions, such that one might expect corresponding essential (or Miransky) scaling of observables near the phase transition [116–123] with universal powerlaw corrections [124]; see also [43,55,56]. On the other hand, the spectra on the two sides of the phase transition share some similarities: on both sides, the fermion and the photon fields are massless; there is a massive (but presumably unstable) vector excitation on the quasiconformal side, while there are a massive “radial” excitation and massless Goldstone bosons on the Lorentz symmetry-breaking side. Near the transition at $N_{f,\text{cr}}^{\text{qc}}$ all these vectorlike degrees of freedom can possibly mix nontrivially which might influence the nature of the transition.

In order to check the scenario suggested above, it appears highly worthwhile to search for vector condensates $\langle \bar{\psi}\gamma_\mu\psi \rangle$ also with other nonperturbative methods in the region above the chiral phase transition $N_f \gtrsim N_{f,\text{cr}}^\chi$. If a vector condensate is found, our work suggests the existence of a further transition to the quasiconformal phase at $N_{f,\text{cr}}^{\text{qc}} > N_{f,\text{cr}}^\chi$.

IX. CONCLUSIONS

In the present work we have studied the many-flavor phase diagram of QED₃ by analyzing the RG fixed-point structure of the theory. In addition to the asymptotically free Gaussian fixed point, the fixed-point structure of QED₃ shares similarities with that of the three-dimensional Thirring model which has the same global chiral/flavor symmetries.

For large flavor numbers $N_f > N_{f,\text{cr}}^{\text{qc}}$, the screening property of fermionic fluctuations induces an IR attractive, quasiconformal, fixed point in the gauge sector, which in the fermionic sector corresponds to a slightly shifted Gaussian fixed point, implying that the fermionic system remains attracted by this fixed point. For large N_f , the system is in a quasiconformal phase and remains massless in complete agreement with expectations and literature results. If this large- N_f phase described a condensed-matter system, the existence of the quasiconformal fixed point would indicate a so-called algebraic-Fermi-liquid phase [11], with striking consequences to the electronic, optical, and thermodynamic experimental observables. Such a material would be one of the very rare examples above 1 + 1 dimensions and without disorder or magnetic field, which exhibit genuine non-Fermi liquid behavior. If QED₃ is indeed an effective theory for the superconductor-insulator transition in the cuprates, our result of a large $N_{f,\text{cr}}^{\text{qc}} > 2$, however, supports the scenario that cuprates at $T = 0$ are not in the quasiconformal phase, and there is no algebraic-Fermi-liquid behavior for any doping of the cuprates.

Lowering N_f , the system approaches the lower end of the “quasiconformal window” at $N_{f,\text{cr}}^{\text{qc}}$ which is characterized by a merger of the Gaussian and the “Thirring” fixed

point in the fermionic interactions. This mechanism is similar to the one discovered in four-dimensional many-flavor QCD [54–56], which gives rise to BKT-type scaling behavior [121,123,124]. As an important difference, we observe the possibility in QED₃ that the RG flow can remain dominated by the vector channel for N_f slightly below $N_{f,\text{cr}}^{\text{qc}}$. Only for even smaller N_f , the chiral channel eventually takes over such that the theory can definitely be expected to be in the chirally broken phase with massive fermions.

If these findings persist beyond the approximations underlying our analysis, the phase diagram of QED₃ along the many-flavor direction can exhibit more phases than previously anticipated. In between the chirally broken phase for $N_f < N_{f,\text{cr}}^{\text{z}}$ and the quasiconformal phase for $N_f > N_{f,\text{cr}}^{\text{qc}}$, there can exist a vector-channel dominated phase provided that $N_{f,\text{cr}}^{\text{z}} < N_{f,\text{cr}}^{\text{qc}}$. If the vector channel becomes critical, this phase could be characterized by a Lorentz-breaking vector condensate and a corresponding excitation spectrum with photonlike Goldstone bosons as well as a massive radial-type mode.

From a technical perspective, we have discovered that a Fierz-complete set of fermionic interactions is a mandatory ingredient for reliably estimating quantities such as $N_{f,\text{cr}}^{\text{qc}}$. Simple projections onto seemingly physically relevant channels can imply a complete loss of quantitative control. This result may inspire corresponding improvements in other analytic approximation schemes used in the literature. A similar word of caution applies to lattice approaches: as Fierz completeness is a statement about the exact realization of the $U(2N_f)$ flavor symmetry of the model, a lattice formulation that is not guaranteed to preserve the full continuum flavor symmetry may simply simulate a different continuum model with possibly very different values of $N_{f,\text{cr}}^{\text{qc}}$. Indeed, a previous RG approach to such a QED₃ theory in the presence of $U(2N_f)$ -symmetry breaking interactions revealed that those perturbatively irrelevant interactions may become relevant for strong gauge coupling, significantly affecting the corresponding predictions for $N_{f,\text{cr}}^{\text{qc}}$ [29]. Also, while certainly tempting, it is thus premature to speculate on possible consequences of the new vector-channel-dominated phase, which we predict for $N_{f,\text{cr}}^{\text{z}} < N_f < N_{f,\text{cr}}^{\text{qc}}$, on the cuprate phase diagram: Even if this new phase reached all the way down to the physical flavor number $N_f = 2$ (i.e., if $N_{f,\text{cr}}^{\text{z}}$ was smaller than 2, in contrast to most of the previous findings, and also to our estimate), the actual cuprate system does not have the full $U(2N_f)$ symmetry and it is momentarily unclear how the presence of the symmetry-breaking short-range interactions will affect the many-flavor phase diagram in QED₃ and the existence of the vector-channel-dominated intermediate phase. This deserves further investigation.

From a quantitative viewpoint, our result for $N_{f,\text{cr}}^{\text{qc}}$ is still rather strongly affected by artificial regularization-scheme dependencies. This may hint to the insufficient resolution

of momentum dependencies of the vertices which in our work is only estimated by an overall RG scale. We consider Eq. (40) to represent our best estimate: $N_{f,\text{cr}}^{\text{qc}} \approx 4.1 \dots 10.0$.

For the chiral-critical flavor number, our results are compatible with those of the most advanced DSE studies, suggesting $N_{f,\text{cr}}^{\text{z}} \approx 4$. Hence, the window of theories in the vector-channel-dominance phase could be finite and include theories with integer N_f .

However, under the assumption that the gauge contributions to the approach to criticality stay subdominant, we conjecture the chiral-critical flavor number of QED₃ and the 3D Thirring model to be identical. A recent study of the 3D Thirring model suggests that $N_{f,\text{cr}}^{\text{z,Thirring}} \approx 5.1$; see Ref. [62]. In the light of our QED₃-Thirring conjecture and the approximation involved in our computation, we can therefore not exclude the possibility that $N_{f,\text{cr}}^{\text{z}}$ and $N_{f,\text{cr}}^{\text{qc}}$ are so close to each other that the vector-dominance phase does not include a system with integer N_f . While it is certainly not inconceivable that $N_{f,\text{cr}}^{\text{z}}$ and $N_{f,\text{cr}}^{\text{qc}}$ are in fact identical, we see no natural reason for this coincidence to hold. Of course, a verification and exact determination of the phase boundaries of the many-flavor phase diagram requires more elaborate studies in the future, ideally by using various different theoretical approaches. In any case, the present work points to a so far overlooked new intermediate phase and may therefore help to better our understanding of the dynamics underlying low-dimensional fermionic field theories and the corresponding strongly correlated condensed-matter systems.

ACKNOWLEDGMENTS

The authors thank Jürgen Berges, Christian S. Fischer, and Igor F. Herbut for useful discussions and Zan Pan for helpful comments on the manuscript. J. B. and D. R. acknowledge support by the Deutsche Forschungsgemeinschaft (DFG) under Grant No. BR 4005/2-1 and by HIC for FAIR within the LOEWE program of the State of Hesse. Moreover, J. B. acknowledges support by the DFG under Grant No. SFB 634. H. G. acknowledges support by the DFG under Grants No. Gi 328/5-2 (Heisenberg program), and No. Gi 328/6-2 (FOR 723). L. J. is supported by the DFG under Grants No. JA 2306/1-1, No. FOR 723, and No. GRK 1523.

APPENDIX A: IRREDUCIBLE REPRESENTATION

Though the reducible representation using 4-component Dirac spinors ψ^a , $a = 1, \dots, N_f$ has its merits from the viewpoint of applications in condensed-matter systems, some aspects become more transparent in the irreducible representation using 2-component spinors χ^i , $i = 1, \dots, 2N_f$. In our conventions, the transition between these representations can be defined using the projector

$$P_{L,R}^{(45)} = \frac{1}{2}(1 \pm \gamma_{45}). \quad (\text{A1})$$

Decomposing χ^i into (χ^a, χ^{a+N_f}) , for $a = 1, \dots, N_f$, we introduce the χ subcomponents by

$$P_L \psi^a = \frac{1}{\sqrt{2}} \chi^a \otimes \begin{pmatrix} 1 \\ i \end{pmatrix}, \quad \bar{\psi}^a P_L = \frac{1}{\sqrt{2}} \bar{\chi}^a \otimes (1, -i), \quad (\text{A2})$$

and

$$P_R \psi^a = \frac{1}{\sqrt{2}} \chi^{a+N_f} \otimes \begin{pmatrix} 1 \\ -i \end{pmatrix}, \quad (\text{A3})$$

$$\bar{\psi}^a P_R = -\frac{1}{\sqrt{2}} \bar{\chi}^{a+N_f} \otimes (1, i).$$

In the irreducible representation, the enhanced $U(2N_f)$ symmetry of QED₃ becomes obvious, since

$$\bar{\psi}^a \gamma_\mu \psi^a = \bar{\chi}^i \sigma_\mu \chi^i, \quad i = 1, \dots, 2N_f, \quad (\text{A4})$$

and σ_μ denote the Pauli matrices. Similarly, it is straightforward to show that $\bar{\psi}^a \psi^a = \bar{\chi}^a \chi^a - \bar{\chi}^{a+N_f} \chi^{a+N_f}$ and $\bar{\psi}^a \gamma_{45} \psi^a = \bar{\chi}^i \chi^i$. The latter implies that a mass term of the form $i\tilde{m} \bar{\psi}^a \gamma_{45} \psi^a$ actually preserves the $U(2N_f)$ symmetry. Also, the interaction term $(P)^2$ introduced in the main text in Eq. (5) in this notation indeed becomes the standard Gross-Neveu interaction for two-component spinors.

In the same spirit the nonsinglet interaction channel $(S)^2$ as used in Eq. (10) can be shown to read

$$(S)^2 = 2(\bar{\chi}^i \chi^j)^2 \equiv 2\bar{\chi}^i \chi^j \bar{\chi}^j \chi^i, \quad (\text{A5})$$

where the factor of 2 on the right-hand side motivates the different coupling normalization between the $(V)^2$ and the $(S)^2$ term in Eq. (10).

APPENDIX B: REGULATOR FUNCTIONS

In this appendix, we summarize the regulator functions employed in the present work. For the definition of the regulator functions, it is convenient to introduce so-called regulator shape functions $r_{F,B}$ for the fermions (F) and bosons (B), respectively:

$$R_F(p) = -\not{p} r_F(y) \quad \text{and} \quad R_B(p^2) = p^2 r_B(y), \quad (\text{B1})$$

where $y = p^2/k^2$. Overall, we have used four different regulator functions, namely the Callan-Symanzik regulator R_{CS} with

TABLE II. Numerical values for the threshold functions as obtained from the various regulators employed in this work and listed in Appendix B. Depending on the type of internal lines in the 1PI diagram underlying the different threshold functions, these functions can be written as a sum of three terms: a pure (real-valued) number (\mathcal{N}), a number times η_ψ (2nd row), and a number times η_A (3rd row). Values with an asterisk * depend on the details of the definition of the nonanalytic sharp cutoff.

		R_{CS}	R_{exp}	R_{lin}	R_{SC}
$l_1^{(F)}$	\mathcal{N}	$\frac{\pi}{2}$	$\frac{\sqrt{\pi}}{2}$	$\frac{2}{3}$	1
	$\sim \eta_\psi$	-0.858407	-0.306377	$-\frac{1}{6}$	-
$l_{1,1}^{(F,B)}$	\mathcal{N}	$\frac{\pi}{4}$	1.03828	$\frac{4}{3}$	1
	$\sim \eta_\psi$	-0.237463	-0.208436	$-\frac{1}{6}$	-
	$\sim \eta_A$	$-\frac{\pi}{16}$	-0.170823	$-\frac{2}{15}$	-
$l_{2,1}^{(F,B)}$	\mathcal{N}	$\frac{3\pi}{16}$	1.02494	2	1
	$\sim \eta_\psi$	-0.126032	-0.153062	$-\frac{1}{6}$	-
	$\sim \eta_A$	$-\frac{\pi}{16}$	-0.243833	$-\frac{4}{15}$	-
$m_{2,1}^{(F,B)}$	\mathcal{N}	$\frac{2}{3}$	0.821746	1	$\frac{2}{3}$
	$\sim \eta_\psi$	-0.077618	-0.043037	0	-
	$\sim \eta_A$	$-\frac{4}{15}$	-0.26131	$-\frac{1}{4}$	-
$\tilde{m}_{1,1}^{(F,B)}$	\mathcal{N}	1	1.23262	$\frac{3}{2}$	1*
	$\sim \eta_\psi$	-0.214602	-0.19434	$-\frac{1}{6}$	-
	$\sim \eta_A$	$-\frac{1}{3}$	-0.298558	$-\frac{1}{4}$	-

$$r_F(y) = \sqrt{\frac{y+1}{y}} - 1, \quad r_B(y) = \frac{1}{y}, \quad (\text{B2})$$

the exponential regulator R_{exp} with

$$r_F(y) = \frac{1}{\sqrt{1-e^{-y}}} - 1, \quad r_B(y) = \frac{1}{e^y - 1}, \quad (\text{B3})$$

and the linear regulator R_{lin} ; see Refs. [108–110], with

$$r_F(y) = \left(\frac{1}{\sqrt{y}} - 1 \right) \theta(1-y), \quad (\text{B4})$$

$$r_B(y) = \left(\frac{1}{y} - 1 \right) \theta(1-y), \quad (\text{B5})$$

and the so-called sharp-cutoff regulator with

$$r_F(y) = \lim_{b \rightarrow \infty} \sqrt{1 + \frac{1}{y^b}} - 1, \quad r_B(y) = \lim_{b \rightarrow \infty} \frac{1}{y^b}. \quad (\text{B6})$$

Note that the sharp-cutoff regulator has to be handled with care as it requires a definite prescription of the order of the various limiting processes involved, in order to avoid ambiguities in the evaluation of the loop integrals. In particular, this is the case for the threshold function $\tilde{m}_{1,1}^{(F,B)}$; cf. also the RG equations in Ref. [29]. These artifacts of the sharp-cutoff scheme are well known; see,

e.g., the discussion of the BKT-phase transition in [92], Chapter 6.4. In Table II, we list the numerical values for the threshold functions as obtained from the various employed regulators.

APPENDIX C: RG FLOW OF Z_A

We briefly summarize the derivation of the equation for the anomalous dimension of the photon, $\eta_A = -\partial_t \ln Z_A$. We begin by rewriting the Wetterich Eq. (19) as follows:

$$\partial_t \Gamma_k = \frac{1}{2} \text{STr} \tilde{\partial}_t \ln (\Gamma_k^{(2)} + R_k), \quad (\text{C1})$$

where $\tilde{\partial}_t$ denotes a formal derivative acting only on the regulator function R_k . The representation (C1) of the Wetterich equation is a convenient starting point for the computation of both the fermionic RG flows (see, e.g., Ref. [83] for a detailed introduction) as well as for the anomalous dimensions. In order to calculate the flow equation for Z_A , we decompose the inverse regularized propagator $\Gamma_k^{(2)}$ on the right-hand side of the flow equation

into a field-independent (\mathcal{P}_k) and a field-dependent (\mathcal{F}_k) part,

$$\Gamma_k^{(2)} + R_k = \mathcal{P}_k + \mathcal{F}_k. \quad (\text{C2})$$

The flow equation can then be decomposed in powers of the fields:

$$\partial_t \Gamma_k = \frac{1}{2} \text{STr} \left\{ \tilde{\partial}_t \sum_{n=1}^{\infty} \frac{(-1)^{n+1}}{n} (\mathcal{P}_k^{-1} \mathcal{F}_k)^n \right\}. \quad (\text{C3})$$

On the right-hand side we have dropped a field-independent term which is of no relevance for our present study. The powers of $\mathcal{P}_k^{-1} \mathcal{F}_k$ can be calculated by straightforward matrix multiplications. It is then straightforward to project the various terms from the expansion appearing on the right-hand side of Eq. (C3) onto our *Ansatz* for the effective action. To the flow of Z_A only the second term of the expansion contributes and we find

$$\eta_A = -\frac{1}{2Z_A} \left\{ \frac{P_{\mu\nu}^T(p)}{p^2} \left(\int \frac{d^3q}{(2\pi)^3} \frac{\tilde{\delta}}{\delta A_\mu(-p)} \frac{1}{2} \text{STr} \left[\tilde{\partial}_t \frac{(-1)}{2} (\mathcal{P}_k^{-1} \mathcal{F}_k)^2 \right] \frac{\tilde{\delta}}{\delta A_\nu(q)} \Big|_{\tilde{\psi}=\psi=0, A_\mu=0} \right. \right. \\ \left. \left. - \int \frac{d^3q}{(2\pi)^3} \frac{\tilde{\delta}}{\delta A_\mu(-p')} \frac{1}{2} \text{STr} \left[\tilde{\partial}_t \frac{(-1)}{2} (\mathcal{P}_k^{-1} \mathcal{F}_k)^2 \right] \frac{\tilde{\delta}}{\delta A_\nu(q)} \Big|_{\tilde{\psi}=\psi=0, A_\mu=0, p'=0} \right) \right\}_{p^2=\zeta^2 k^2}, \quad (\text{C4})$$

where we have used the transversal projector $P_{\mu\nu}^T(p) = \delta_{\mu\nu} - \frac{p_\mu p_\nu}{p^2}$. The second term corresponds to the subtraction of the zero-momentum limit of the regularized flow which is constrained by the regulator-modified Ward identity. In this way, the transversal projection entering the definition of η_A satisfies the standard Ward identity at all scales. This construction is based on the implicit assumption that the longitudinal

and the transversal part of the photon propagator do not differ by nonanalyticities at small momenta. From this expression, we then obtain

$$\eta_A = 8v_3 N_f e^2 \mathcal{L}_1^{(F)}, \quad (\text{C5})$$

where $v_3 = 1/(8\pi)^2$ and

$$\mathcal{L}_1^{(F)}(\eta_\psi; \zeta) \equiv \mathcal{L}_1^{(F)} = \frac{1}{\zeta^2} \int_0^\infty dy \left\{ \frac{2}{3} \frac{\partial_t r_\psi(y) - \eta_\psi r_\psi(y)}{\sqrt{y} [1 + r_\psi(y)]^3} - \frac{1}{2} \int_{-1}^1 dx \frac{\sqrt{y} x^2 - \zeta x}{y - 2\zeta x \sqrt{y} + \zeta^2} \left[\frac{[\partial_t r_\psi](y) - \eta_\psi r_\psi(y)}{[1 + r_\psi(y)]^2 [1 + r_\psi(y - 2\zeta x \sqrt{y} + \zeta^2)]} \right. \right. \\ \left. \left. + \frac{[\partial_t r_\psi](y - 2\zeta x \sqrt{y} + \zeta^2) - \eta_\psi r_\psi(y - 2\zeta x \sqrt{y} + \zeta^2)}{[1 + r_\psi(y)][1 + r_\psi(y - 2\zeta x \sqrt{y} + \zeta^2)]^2} \right] \right\}. \quad (\text{C6})$$

Here, we have introduced $y = q^2/k^2$ for convenience and $x = \cos \vartheta$.

- [1] S. Weinberg, *Phys. Rev. D* **19**, 1277 (1979).
- [2] B. Holdom, *Phys. Rev. D* **24**, 1441 (1981).
- [3] D. K. Hong, S. D. H. Hsu, and F. Sannino, *Phys. Lett. B* **597**, 89 (2004).
- [4] F. Sannino and K. Tuominen, *Phys. Rev. D* **71**, 051901 (2005).
- [5] D. D. Dietrich, F. Sannino, and K. Tuominen, *Phys. Rev. D* **72**, 055001 (2005).
- [6] D. D. Dietrich and F. Sannino, *Phys. Rev. D* **75**, 085018 (2007).
- [7] F. Sannino, *Acta Phys. Pol. B* **40**, 3533 (2009).
- [8] A. Cortijo, F. Guinea, and M. A. Vozmediano, *J. Phys. A* **45**, 383001 (2012).
- [9] O. Vafek and A. Vishwanath, *Annu. Rev. Condens. Matter Phys.* **5**, 83 (2014).
- [10] M. Franz and Z. Tesanovic, *Phys. Rev. Lett.* **87**, 257003 (2001).
- [11] M. Franz, Z. Tesanovic, and O. Vafek, *Phys. Rev. B* **66**, 054535 (2002).
- [12] I. F. Herbut, *Phys. Rev. Lett.* **88**, 047006 (2002).
- [13] I. F. Herbut, *Phys. Rev. B* **66**, 094504 (2002).
- [14] Z. Tesanovic, O. Vafek, and M. Franz, *Phys. Rev. B* **65**, 180511 (2002).
- [15] N. Mavromatos and J. Papavassiliou, *Recent Res. Dev. Phys. Chem.* **5**, 369 (2004).
- [16] I. F. Herbut, *Phys. Rev. Lett.* **94**, 237001 (2005).
- [17] T. Appelquist, D. Nash, and L. C. R. Wijewardhana, *Phys. Rev. Lett.* **60**, 2575 (1988).
- [18] D. Nash, *Phys. Rev. Lett.* **62**, 3024 (1989).
- [19] M. R. Pennington and D. Walsh, *Phys. Lett. B* **253**, 246 (1991).
- [20] D. Atkinson, P. Johnson, and P. Maris, *Phys. Rev. D* **42**, 602 (1990).
- [21] D. Curtis, M. Pennington, and D. Walsh, *Phys. Lett. B* **295**, 313 (1992).
- [22] P. Maris, *Phys. Rev. D* **52**, 6087 (1995).
- [23] K.-I. Kondo, T. Ebihara, T. Iizuka, and E. Tanaka, *Nucl. Phys.* **B434**, 85 (1995).
- [24] P. Maris, *Phys. Rev. D* **54**, 4049 (1996).
- [25] I. Aitchison, N. Mavromatos, and D. McNeill, *Phys. Lett. B* **402**, 154 (1997).
- [26] T. Appelquist, A. G. Cohen, and M. Schmaltz, *Phys. Rev. D* **60**, 045003 (1999).
- [27] V. Gusynin and M. Reenders, *Phys. Rev. D* **68**, 025017 (2003).
- [28] C. S. Fischer, R. Alkofer, T. Dahm, and P. Maris, *Phys. Rev. D* **70**, 073007 (2004).
- [29] K. Kaveh and I. F. Herbut, *Phys. Rev. B* **71**, 184519 (2005).
- [30] K.-I. Kubota and H. Terao, *Prog. Theor. Phys.* **105**, 809 (2001).
- [31] S. Hands, J. Kogut, and C. Strouthos, *Nucl. Phys.* **B645**, 321 (2002).
- [32] S. Hands, J. Kogut, L. Scorzato, and C. Strouthos, *Phys. Rev. B* **70**, 104501 (2004).
- [33] R. Fiore, P. Giudice, D. Giuliano, D. Marmottini, A. Papa, and P. Sodano, *Phys. Rev. D* **72**, 094508 (2005).
- [34] I. Mitra, R. Ratabole, and H. Sharatchandra, *Mod. Phys. Lett. A* **22**, 297 (2007).
- [35] C. Strouthos and J. B. Kogut, *J. Phys. Conf. Ser.* **150**, 052247 (2009).
- [36] A. Bashir, A. Raya, I. Cloet, and C. Roberts, *Phys. Rev. C* **78**, 055201 (2008).
- [37] R. Fiore, P. Giudice, and A. Papa, *J. High Energy Phys.* **11** (2008) 055.
- [38] A. Bashir, A. Raya, S. Sanchez-Madrigal, and C. Roberts, *Few-Body Syst.* **46**, 229 (2009).
- [39] H.-t. Feng, B. Wang, W.-m. Sun, and H.-s. Zong, *Phys. Rev. D* **86**, 105042 (2012).
- [40] T. Grover, *Phys. Rev. Lett.* **112**, 151601 (2014).
- [41] J. A. Bonnet, C. S. Fischer, and R. Williams, *Phys. Rev. B* **84**, 024520 (2011).
- [42] J. A. Bonnet, C. S. Fischer, and R. Williams, *Prog. Part. Nucl. Phys.* **67**, 245 (2012).
- [43] J. A. Bonnet and C. S. Fischer, *Phys. Lett. B* **718**, 532 (2012).
- [44] C. Popovici, C. Fischer, and L. von Smekal, *Phys. Rev. B* **88**, 205429 (2013).
- [45] H. Gies and L. Janssen, *Phys. Rev. D* **82**, 085018 (2010).
- [46] L. Janssen, PhD thesis, University of Jena, <http://www.db-thueringen.de/servlets/DocumentServlet?id=20856>, 2012.
- [47] G. W. Semenoff, *Phys. Rev. Lett.* **53**, 2449 (1984).
- [48] S. Hands and C. Strouthos, *Phys. Rev. B* **78**, 165423 (2008).
- [49] I. F. Herbut, V. Juricic, and B. Roy, *Phys. Rev. B* **79**, 085116 (2009).
- [50] J. E. Drut and T. A. Lahde, *Phys. Rev. B* **79**, 165425 (2009).
- [51] W. Armour, S. Hands, and C. Strouthos, *Phys. Rev. B* **81**, 125105 (2010).
- [52] V. Gusynin, S. Sharapov, and J. Carbotte, *Int. J. Mod. Phys. B* **21**, 4611 (2007).
- [53] D. Smith and L. von Smekal, *Phys. Rev. B* **89**, 195429 (2014).
- [54] H. Gies and J. Jaeckel, *Eur. Phys. J. C* **46**, 433 (2006).
- [55] J. Braun and H. Gies, *Phys. Lett. B* **645**, 53 (2007).
- [56] J. Braun and H. Gies, *J. High Energy Phys.* **06** (2006) 024.
- [57] J. Hubbard, *Phys. Rev. Lett.* **3**, 77 (1959).
- [58] R. Stratonovich, *Dokl. Akad. Nauk.* **115**, 1097 (1957).
- [59] T. Baier, E. Bick, and C. Wetterich, *Phys. Rev. B* **62**, 15471 (2000).
- [60] H. Gies and C. Wetterich, *Phys. Rev. D* **65**, 065001 (2002).
- [61] J. Jaeckel and C. Wetterich, *Phys. Rev. D* **68**, 025020 (2003).
- [62] L. Janssen and H. Gies, *Phys. Rev. D* **86**, 105007 (2012).
- [63] J. Bjorken, *Ann. Phys. (N.Y.)* **24**, 174 (1963).
- [64] I. Bialynicki-Birula, *Phys. Rev.* **130**, 465 (1963).
- [65] G. Guralnik, *Phys. Rev.* **136**, B1404 (1964).
- [66] T. Banks and A. Zaks, *Nucl. Phys.* **B184**, 303 (1981).
- [67] P. Kraus and E. Tomboulis, *Phys. Rev. D* **66**, 045015 (2002).
- [68] C. Wetterich, *Phys. Lett. B* **301**, 90 (1993).
- [69] P. Strack, S. Takei, and W. Metzner, *Phys. Rev. B* **81**, 125103 (2010).
- [70] L. F. Abbott, *Nucl. Phys.* **B185**, 189 (1981).
- [71] L. Abbott, *Acta Phys. Pol. B* **13**, 33 (1982).
- [72] W. Dittrich and M. Reuter, *Lect. Notes Phys.* **244**, 1 (1986).

- [73] M. Reuter and C. Wetterich, *Nucl. Phys.* **B417**, 181 (1994).
- [74] M. Reuter and C. Wetterich, *Phys. Rev. D* **56**, 7893 (1997).
- [75] H. Gies, *Phys. Rev. D* **66**, 025006 (2002).
- [76] H. Gies and J. Jaeckel, *Phys. Rev. Lett.* **93**, 110405 (2004).
- [77] H. Gies, *Lect. Notes Phys.* **852**, 287 (2012).
- [78] R. D. Pisarski, *Phys. Rev. D* **29**, 2423 (1984).
- [79] U. Ellwanger, M. Hirsch, and A. Weber, *Z. Phys. C* **69**, 687 (1996).
- [80] U. Ellwanger, M. Hirsch, and A. Weber, *Eur. Phys. J. C* **1**, 563 (1998).
- [81] D. F. Litim and J. M. Pawłowski, *Phys. Lett. B* **435**, 181 (1998).
- [82] O. Lauscher and M. Reuter, *Phys. Rev. D* **65**, 025013 (2001).
- [83] J. Braun, *J. Phys. G* **39**, 033001 (2012).
- [84] S. Pokorski, *Gauge Field Theories* (Cambridge University Press, Cambridge, 1987).
- [85] U. Ellwanger, *Phys. Lett. B* **335**, 364 (1994).
- [86] D. F. Litim and J. M. Pawłowski, arXiv:hep-th/9901063.
- [87] D. F. Litim and J. M. Pawłowski, *J. High Energy Phys.* **09** (2002) 049.
- [88] J. M. Pawłowski, *Ann. Phys. (Amsterdam)* **322**, 2831 (2007).
- [89] H. Gies, J. Jaeckel, and C. Wetterich, *Phys. Rev. D* **69**, 105008 (2004).
- [90] F. Freire, D. F. Litim, and J. M. Pawłowski, *Phys. Lett. B* **495**, 256 (2000).
- [91] C. S. Fischer and H. Gies, *J. High Energy Phys.* **10** (2004) 048.
- [92] I. F. Herbut, *A Modern Approach to Critical Phenomena* (Cambridge University Press, Cambridge, 2007).
- [93] J. Berges, N. Tetradis, and C. Wetterich, *Phys. Rep.* **363**, 223 (2002).
- [94] H. Gies and C. Wetterich, *Phys. Rev. D* **69**, 025001 (2004).
- [95] D. Mesterhazy, J. Berges, and L. von Smekal, *Phys. Rev. B* **86**, 245431 (2012).
- [96] S. Christofi, S. Hands, and C. Strouthos, *Phys. Rev. D* **75**, 101701 (2007).
- [97] M. Gomes, R. Mendes, R. Ribeiro, and A. da Silva, *Phys. Rev. D* **43**, 3516 (1991).
- [98] D. K. Hong and S. H. Park, *Phys. Rev. D* **49**, 5507 (1994).
- [99] T. Itoh, Y. Kim, M. Sugiura, and K. Yamawaki, *Prog. Theor. Phys.* **93**, 417 (1995).
- [100] M. Sugiura, *Prog. Theor. Phys.* **97**, 311 (1997).
- [101] K.-I. Kondo, *Nucl. Phys.* **B450**, 251 (1995).
- [102] S. Kim and Y. Kim, arXiv:hep-lat/9605021.
- [103] L. Del Debbio, S. Hands, and J. Mehegan (UKQCD Collaboration), *Nucl. Phys.* **B502**, 269 (1997).
- [104] S. Hands and B. Lucini, *Phys. Lett. B* **461**, 263 (1999).
- [105] L. Rosa, P. Vitale, and C. Wetterich, *Phys. Rev. Lett.* **86**, 958 (2001).
- [106] F. Hofling, C. Nowak, and C. Wetterich, *Phys. Rev. B* **66**, 205111 (2002).
- [107] J. Braun, H. Gies, and D. D. Scherer, *Phys. Rev. D* **83**, 085012 (2011).
- [108] D. F. Litim, *Phys. Lett. B* **486**, 92 (2000).
- [109] D. F. Litim, *Phys. Rev. D* **64**, 105007 (2001).
- [110] D. F. Litim, *Int. J. Mod. Phys. A* **16**, 2081 (2001).
- [111] T. Goecke, C. S. Fischer, and R. Williams, *Phys. Rev. B* **79**, 064513 (2009).
- [112] C. Vafa and E. Witten, *Commun. Math. Phys.* **95**, 257 (1984).
- [113] K. Kondo and P. Maris, *Phys. Rev. Lett.* **74**, 18 (1995).
- [114] K. Kondo and P. Maris, *Phys. Rev. D* **52**, 1212 (1995).
- [115] C. P. Hofmann, A. Raya, and S. S. Madrigal, *Phys. Rev. D* **82**, 096011 (2010).
- [116] V. L. Berezinskii, *Sov. Phys. JETP* **32**, 493 (1971).
- [117] V. L. Berezinskii, *Sov. Phys. JETP* **34**, 610 (1972).
- [118] J. M. Kosterlitz and D. J. Thouless, *J. Phys. C* **6**, 1181 (1973).
- [119] T. Appelquist, J. Terning, and L. Wijewardhana, *Phys. Rev. Lett.* **77**, 1214 (1996).
- [120] R. S. Chivukula, *Phys. Rev. D* **55**, 5238 (1997).
- [121] V. A. Miransky and K. Yamawaki, *Mod. Phys. Lett. A* **04**, 129 (1989).
- [122] T. Appelquist and F. Sannino, *Phys. Rev. D* **59**, 067702 (1999).
- [123] D. B. Kaplan, J.-W. Lee, D. T. Son, and M. A. Stephanov, *Phys. Rev. D* **80**, 125005 (2009).
- [124] J. Braun, C. S. Fischer, and H. Gies, *Phys. Rev. D* **84**, 034045 (2011).